

# Functionalized Microscaffold–Hydrogel Composites Accelerating Osteochondral Repair through Endochondral Ossification

He Zhang, Qian Li, Xiangliang Xu, Siqi Zhang, Yang Chen, Tao Yuan, Ziqian Zeng, Yifei Zhang, Zi Mei, Shuang Yan, Lei Zhang\* and Shicheng Wei\*



Cite This: *ACS Appl. Mater. Interfaces* 2022, 14, 52599–52617



Read Online

ACCESS |



Metrics & More



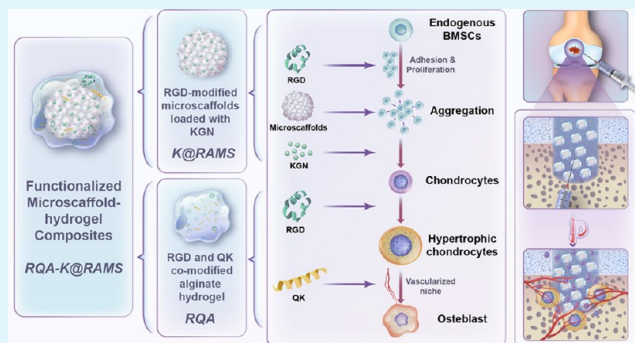
Article Recommendations



Supporting Information

**ABSTRACT:** Osteochondral regeneration remains a key challenge because of the limited self-healing ability of the bone and its complex structure and composition. Biomaterials based on endochondral ossification (ECO) are considered an attractive candidate to promote bone repair because they can effectively address the difficulties in establishing vascularization and poor bone regeneration via intramembranous ossification (IMO). However, its clinical application is limited by the complex cellular behavior of ECO and the long time required for induction of the cell cycle. Herein, functionalized microscaffold–hydrogel composites are developed to accelerate the developmental bone growth process via recapitulating ECO. The design comprises arginine–glycine–aspartic acid (RGD)-peptide-modified microscaffolds loaded with kartogenin (KGN) and wrapped with a layer of RGD- and QK-peptide-comodified alginate hydrogel. These microscaffolds enhance the proliferation and aggregation behavior of the human bone marrow mesenchymal stem cells (hBMSCs); the controlled release of kartogenin induces the differentiation of hBMSCs into chondrocytes; and the hydrogel grafted with RGD and QK peptide facilitates chondrocyte hypertrophy, which creates a vascularized niche for osteogenesis and finally accelerates osteochondral repair in vivo. The findings provide an efficient bioengineering approach by sequentially modulating cellular ECO behavior for osteochondral defect repair.

**KEYWORDS:** osteochondral regeneration, endochondral ossification, bone repair, microscaffold, alginate hydrogel



## 1. INTRODUCTION

Osteochondral injuries due to trauma, sports injuries, or pathological factors, which involve both articular cartilage and subchondral bone tissue, are notorious for being incurable and for seriously affecting the normal activities of human joints, thereby causing not only a huge economic and psychological burden to patients but also consuming a large amount of public medical resources.<sup>1–3</sup> Therefore, the search for an effective osteochondral repair strategy is a pressing clinical and scientific problem. Traditional bone tissue engineering involves directly transforming the mesenchymal stem cells (MSCs) into osteoblasts to form bone matrix through intramembranous ossification (IMO). Although this strategy is promising for clinical applications because of its short induction time and good osteogenesis results in vitro, the engineered constructs created by IMO have extensive matrix deposits on their surfaces that impede material exchange and angiogenesis in the central region of osteogenesis in vivo, ultimately resulting in osteogenesis failure.<sup>4–6</sup> To gain effectiveness and robustness, “developmental engineering” principles were proposed for instructing regeneration through recapitulating the developmental process in vivo by mimicking the natural factors that control cell differentiation

and matrix production.<sup>7,8</sup> In terms of bone development physiology and clinical perspectives, human skeletal development and fracture healing occur mainly through endochondral ossification (ECO).<sup>9</sup> Therefore, ECO-based bone tissue engineering strategies have gained much attention in recent years to address the limitations of traditional bone tissue engineering strategies.<sup>10–12</sup>

ECO begins with the appearance of cell aggregation behavior, characterized by a high rate of cell proliferation, dense cell–cell contacts, and a triggering of the expression of intercellular adhesion molecules, such as N-cadherin, neural cell adhesion molecule (NCAM), and the cell aggregation marker peanut agglutinin (PNA).<sup>13–15</sup> Li et al. found that encapsulation of hMSCs in nanofiber networks to form microspheres could mimic the early agglutination process of cells, with a significant

Received: July 16, 2022

Accepted: November 4, 2022

Published: November 17, 2022



upregulation of chondrogenic and osteogenic-related transcription factors (SOX9 and RUNX2) and significant potential for differentiation into chondrogenic and osteogenic lineages.<sup>16</sup> Subsequently, aggregated MSCs differentiate toward chondrocytes, overexpress a characteristic SOX9-driven genetic program, and secrete an extracellular matrix (ECM) rich in type II collagen (COL2A1) and glycosaminoglycans (GAGs). Finally, chondrocytes proliferate, hypertrophy, and secrete collagen type X (COL10A1) and matrix metalloproteinase-13 (MMP-13).<sup>17</sup> A stable chondrogenic and hypertrophy-inducing microenvironment must be established during this process. Kartogenin (KGN), a small bioactive molecule, possesses excellent biocompatibility and could effectively promote the chondrogenic differentiation of bone mesenchymal stem cells (BMSCs) by breaking the core-binding factor  $\beta$  (CBF- $\beta$ ) and filamin A and promoting the nuclear translocation of CBF- $\beta$  to form a complex with runt-related transcription factor-1 (RUNX1), which enhances the expression of COL2A1 and ACAN.<sup>18</sup> Besides, compared with protein growth factors, KGN shows physicochemical stability in different environments.<sup>19</sup> Teng et al. loaded KGN into PLGA microspheres and effectively promoted cartilage formation in MSCs through the sustained release of KGN.<sup>20</sup> Sodium alginate is a natural polysaccharide polymer, which is a structure similar to the ECM of living tissues, and has been widely used in tissue regeneration, drug delivery, and cell transplantation because of its good biocompatibility, low toxicity, and relatively low cost.<sup>21</sup> Mooney et al. found that sodium alginate hydrogels with stress-relaxing behavior provide a viscoelastic microenvironment for cells and facilitate cartilage matrix formation and chondrocyte proliferation.<sup>22</sup> Arginine–glycine–aspartic acid (RGD), a common sequence that can be found in many matrix proteins, enhances cell adhesion and affects chondrocyte hypertrophy through adhesion patch aggregation and actin fiber contraction.<sup>23</sup> Hypertrophic chondrocytes establish vascularization by releasing vascular endothelial growth factor (VEGF) to induce vascular growth, and their genotype is altered with the expression of pluripotent stem genes such as SOX2, OCT4, and NANOG; finally, they are transformed into osteoblasts to secrete bone matrix.<sup>24,25</sup> QK peptide, a biomimetic polypeptide of VEGF, can bind with VEGF receptor and promote the adhesion and proliferation of vascular endothelial cells.<sup>26,27</sup> Hung et al. used sodium alginate hydrogels grafted with RGD and QK peptides in a 1:1 ratio to encapsulate MSCs and induce osteogenesis in vitro and found a higher level of pro-angiogenic factor secretion and mineralization compared with grafting one peptide alone.<sup>28</sup>

Therefore, use of the physical or chemical clues of biomaterials to regulate the cell behavior in the process of endochondral ossification is the key to bone regeneration. For example, Sun et al. used grafted carboxylated PEGS/PAA hydrogels to build a hypoxic microenvironment by chelating iron ions in situ at the bone defect, thereby activating the hypoxia-inducible factor (HIF)-1 $\alpha$  signaling pathway and suppressing the inflammatory response to improve early chondrocyte differentiation and promote vascularization at a later stage, which triggered the typical ECO.<sup>29</sup> Liu et al. entrapped dexamethasone within biomimetic recombinant human bone morphogenetic protein (rhBMP)-loaded porous mesoporous bioglass scaffolds and regulated their release kinetics to achieve a significant degree of ectopic bone formation through ECO.<sup>30</sup> However, these studies mostly focused on inducing cells to undergo osteogenic repair through ECO using the design of the material and ignoring the fact that cellular

endochondral ossification behavior is a continuous and tight process. What role each component of the material plays in each stage of endochondral ossification remains unclear. Here, we construct functionalized microc scaffold–hydrogel composites, which are made by kartogenin-laden RGD-peptide-modified alginate microc scaffolds (K@RAMS) wrapped with a layer of RGD- and QK-peptide-comodified alginate hydrogel (RQA), and defined as RQA-K@RAMS (Table 1). The RGD-peptide-

**Table 1. Abbreviations and Preparation of Functionalized Microc Scaffold–Hydrogel Composites**

abbreviation	description
UA	unmodified alginate hydrogel
RA	RGD-peptide-modified alginate hydrogel
RQA	RGD- and QK-peptide-comodified alginate hydrogel
K-RQA	KGN-laden RQA
AMS	unmodified alginate microc scaffolds
RAMS	RGD-peptide-modified alginate microc scaffolds
K@RAMS	KGN-laden RAMS
RA-RAMS	RAMS encapsulated in RA
RQA-RAMS	RAMS encapsulated in RQA
K-RQA-RAMS	RAMS encapsulated in KGN-laden RQA
RQA-K@RAMS	K@RAMS encapsulated in RQA

modified alginate microc scaffolds (RAMS) encourage stem cell proliferation and aggregation, the KGN-controlled release from RAMS creates a consistent and stable chondrogenic induction microenvironment, and then the RQA grafted with RGD and QK peptides promotes chondrocyte proliferation and hypertrophy and attracts vascular endothelial cells to migrate and establish a vascularized niche in vivo, thus achieving a full-stage regulation and acceleration of cellular ECO behavior and promoting osteochondral repair effects.

## 2. MATERIALS AND METHODS

**2.1. Materials.** Sodium alginate with high mannuronic acid content (G/M  $\approx$  0.64), calcium chloride, and calcium sulfate powder were purchased from Sigma-Aldrich (St. Louis, USA). 2-(*N*-Morpholino) ethanesulfonic acid (MES), *N*-hydroxy-sulfosuccinimide (sulfo-NHS), and 1-(3-dimethylaminopropyl)-3-ethylcarbodiimide (EDC) were obtained from Aladdin Reagent Co. Ltd. (Shanghai, China). The RGD peptide (GGGGRGDASSP sequence), QK (KLTWQELYQLKYKGI sequence), and the fluorescein isothiocyanate (FITC)-labeled QK were purchased from Dangang Biological Technology Co. Ltd. (Wuhan, China), and all the peptides were synthesized by a batch-wise Fmoc-polyamide method to achieve greater than 98% purity.

**2.2. Peptide Functionalization to Alginate.** As reported previously,<sup>31</sup> the RGD (RA) and QK-functionalized alginate (QA) used to promote cell adhesion and angiogenesis was prepared by the carbodiimide chemistry method. Briefly, EDC and sulfo-NHS were reacted with alginate solution in 0.1 M MES buffer to form a stable intermediate, RGD/QK was added to the solution, and the resulting mixture was allowed to react at 25 °C for 12 h. The final RGD/QK concentration was 1 mM. Following the peptide modification, the alginate was dialyzed (3.5 kDa), sterile-filtered (0.22  $\mu$ m), and freeze-dried. The RGD- and QK-peptide-comodified sodium alginate (RQA) was prepared by mixing RA and QA at a volume ratio of 1:1.

**2.3. Preparation of Alginate Hydrogels.** The unmodified alginate hydrogel (UA) and RQA hydrogel were prepared by mixing calcium sulfate slurry (1.22 M in deionized water) with UA or RQA using Luer-lock syringes, which were injected into a mold (diameter, 5 mm; height, 2 mm) and cross-linked for 15 min.

**2.4. Fabrication of KGN-Laden Alginate Microc Scaffolds (K@RAMS).** As shown in Figure 1A, 1.5 g of RGD-modified alginate (RA) was dissolved completely in 100 mL of deionized water (pH 7.4) to

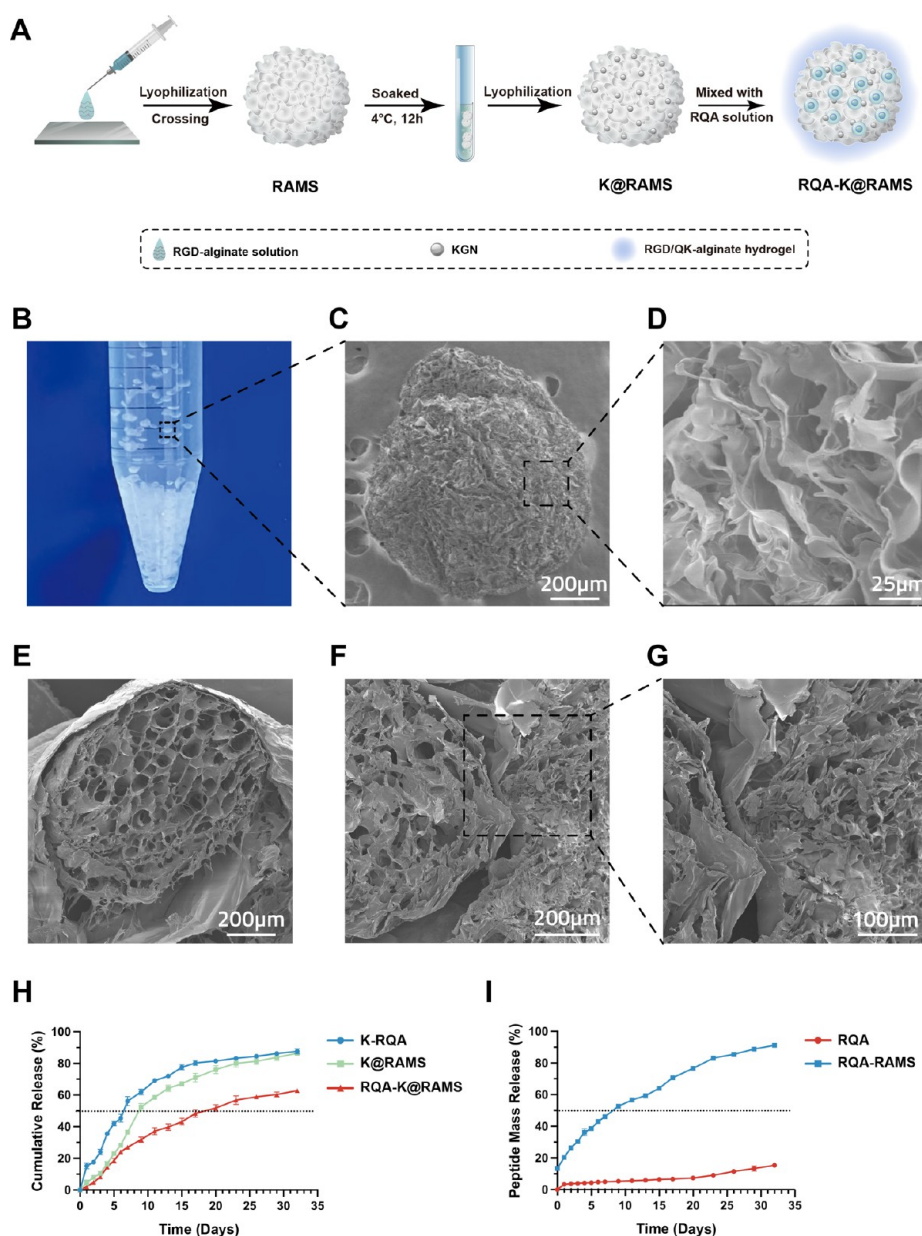


**Figure 1.** Characterization of RQA-K@RAMS and release profiles of KGN and QK from various matrices. (A) Schematic diagram of RQA-K@RAMS preparation. (B) Photographs of K@RAMS. (C,D) Scanning electron microscopy (SEM) images of K@RAMS. (E–G) SEM images of RQA-K@RAMS. (H) KGN release profiles of K-RQA, K@RAMS, and RQA-K@RAMS. (I) The quantitative assessment of FITC-QK of RQA hydrogel and RQA-RAMS over a long incubation period (32 days). The dashed line represents the time required for 50% release of KGN or QK peptide. All data represent the mean  $\pm$  SD ( $n = 3$ ). Scale bar = 200  $\mu\text{m}$ . RQA represents RGD- and QK-peptide-comodified alginate hydrogel; RAMS represents RGD-peptide-modified alginate microscaffolds; RQA-RAMS represents RAMS encapsulated in RQA; K@RAMS represents KGN-laden RAMS; K-RQA represents KGN-laden RQA; RQA-K@RAMS represents K@RAMS encapsulated in RQA.

form alginate aqueous solution, and microdroplets were generated using a syringe with a blunt needle (32 G). The alginate microscaffolds (RAMS) were prepared by lyophilizing the microdroplets immediately after being dropped onto the Teflon plate, cross-linking them with sterile 1%  $\text{CaCl}_2$  solution, and immersing them in deionized water for 3 days before lyophilizing again. The KGN-laden RGD-peptide-modified alginate microscaffolds (K@RAMS) were obtained by soaking RAMS in KGN solution for 12 h and then lyophilization. The final concentration of KGN in the alginate microscaffolds–hydrogel composite system was 0.3  $\text{mg L}^{-1}$ .

**2.5. Fabrication of KGN-Laden Alginate Microscaffold–Hydrogel Composites (RQA-K@RAMS).** The hydrogel around each microscaffold was self-cross-linked by the residual  $\text{Ca}^{2+}$  on the surface of the microscaffolds. Briefly, the RQA-K@RAMS were

prepared by sequentially mixing 200  $\mu\text{L}$  of PBS and 200  $\mu\text{L}$  of RQA into syringes containing K@RAMS through a female–female Luer-lock coupler and repeatedly pushing to make full contact. Afterward, the mixture was cross-linked for 10 min to obtain RQA-K@RAMS that could be extruded from the syringe.

**2.6. Characterization of the Scaffolds.** SEM (S-4800; Hitachi, Japan) was used to measure the size and observe the porous structures of the K@RAMS and RQA-K@RAMS. The release kinetics of the FITC-QK peptide from RQA and RQA-RAMS were determined using a fluorescence microplate reader (SpectraMax MS; Molecular Devices, USA) at the wavelength of 488 nm. Each sample was immersed in PBS (pH 7.4, 37  $^\circ\text{C}$ ) for up to 35 days. At the predetermined time points, 100  $\mu\text{L}$  of supernatant was collected for quantification of the peptide released in the solution. The peptide concentration was calculated by

comparison with the established standard curve. The release kinetics of KGN were determined using high-performance liquid chromatography (HPLC; 1260 Infinity; Agilent, USA). Briefly, KGN encapsulated in RQA hydrogel (K-RQA), K@RAMS, and RQA-K@RAMS were first placed in PBS solution and then in a 37 °C shaking incubator at 100 rpm. The supernatant was collected, and the KGN content was measured by HPLC at the predetermined time points. The initial total amount of KGN at the time of KGN encapsulation was M1, and the KGN content of the supernatant was measured with a value of M2; the release rate of KGN =  $M2/M1 \times 100\%$ .

**2.7. Cell Culture and Seeding on Scaffolds.** hBMSCs (Carlsbad, CA, USA) were maintained in high glucose Dulbecco's modified Eagle medium (DMEM; Hyclone, USA) supplemented with 10% fetal bovine serum (Gibco, NY, USA) and 1% penicillin/streptomycin (Gibco) and used at passage 5. For cell-loaded sodium alginate hydrogels, hBMSCs in the dish were trypsinized with 0.05% trypsin/EDTA (Gibco) and resuspended in serum-free medium. Then, a Luer-lock syringe was used to thoroughly mix the cell suspension with unmodified alginate solutions ( $3 \times 10^6$  cells per mL in alginate) and then quickly mix with calcium sulfate before injection into a mold. For the cell-loaded alginate microscaffolds, the cell suspension was added to the syringe with sodium alginate microscaffolds, which were mixed thoroughly and then placed in the incubator for 30 min. For the cell-loaded alginate microsphere-hydrogel composite, a syringe with sodium alginate solution was mixed with the cell-loaded alginate microscaffolds through a female-female Luer-lock coupler. Afterward, the mixture was cross-linked for 10 min to obtain the cell-loaded alginate microsphere-hydrogel composite that could be extruded from the syringe. The samples were transferred to a low-viscosity 24-well plate (Costar) and immersed in 1.5 mL proliferation medium.

**2.8. Proliferation and Aggregation of hBMSCs on Scaffolds.** The CCK-8 assay was used to evaluate the viability of hBMSCs. Briefly, after incubation for 1, 3, and 7 days, 10% CCK-8 reagent was added to each well and allowed to react for 4 h. The absorbance value of the supernatant optical density (OD) was measured using a microplate reader (SpectraMax M5) at 450 nm. The morphology and aggregation behavior of hBMSCs cultured on various scaffolds was observed by confocal laser scanning microscopy (CLSM; A1R-si, Nikon, Japan). Briefly, after incubation for 3 days, the samples were fixed with 4% (w/v) paraformaldehyde (Hyclone, Logan, UT, USA) for 30 min, they were washed three times with PBS, and then they were permeabilized with 0.1% (v/v) Triton X-100 (Sigma-Aldrich) for 15 min. After that, the samples were washed three times with PBS and then incubated with primary antibodies (NCAM1 = Abcam, ab133345; N-cadherin = Abcam, ab98952; PNA = vector laboratories RL-1072-5; SOX9 = Abcam ab238053; Integrin  $\beta$ 1 = Abcam, ab183666), at 4 °C overnight. After three washes with PBS, the samples were incubated with secondary antibodies at a dilution of 1:500 for 2 h in the dark at room temperature and stained with 5 mg mL<sup>-1</sup> FITC-phalloidin solution (Sigma) and 10 mg mL<sup>-1</sup> DAPI solution (Sigma-Aldrich). The stained samples were visualized immediately by confocal laser scanning microscopy (CLSM). Quantitative analysis of the immunofluorescence staining was analyzed using ImageJ software (NIH, Bethesda, USA).

**2.9. Induction of Endochondral Ossification of hBMSCs In Vitro.** Cell-loaded various scaffolds were incubated in proliferation medium for 3 days to allow hBMSCs proliferation and aggregation. Then, followed by the in vitro endochondral ossification induction protocol,<sup>32</sup> the cell-loaded scaffolds were first cultured for 3 weeks in chondrogenic medium (high glucose DMEM; 100 nM dexamethasone; 50  $\mu$ g mL<sup>-1</sup> ascorbic acid; 50  $\mu$ g mL<sup>-1</sup> L-proline; 100  $\mu$ g mL<sup>-1</sup> sodium pyruvate; 1% ITS+; 1% P/S; 10 ng mL<sup>-1</sup> TGF- $\beta$ 3; 1 mM CaCl<sub>2</sub>). For the subsequent 2 weeks, the medium was changed to hypertrophic medium (high glucose DMEM; 1 nM dexamethasone; 50  $\mu$ g mL<sup>-1</sup> ascorbic acid; 50  $\mu$ g mL<sup>-1</sup> L-proline; 100  $\mu$ g mL<sup>-1</sup> sodium pyruvate; 1% ITS+; 1% P/S; 50  $\mu$ g mL<sup>-1</sup> L-thyroxine; 5 mM  $\beta$ -glycerophosphate; 1 mM CaCl<sub>2</sub>).

**2.10. Immunofluorescence Analysis.** Cell morphology, cartilage, and hypertrophic cartilage-related protein expression were analyzed by CLSM when the cell-scaffold complexes were cultured up to 2 weeks and 5 weeks. The primary antibodies used included COL2A1 (1:200,

Abcam, ab34712), ACAN (1:50, Abcam, ab3778), COL10A1 (1:1000, Abcam, ab49945), and MMP13 (1:100, Abcam, 39012).

**2.11. Histological Staining and Evaluation of In Vitro Samples.** The in vitro induction of the cell-scaffold complexes at 2 and 5 weeks were fixed with 4% paraformaldehyde (Solarbio, China) overnight. Then, the specimens were dehydrated with gradient ethanol, embedded in paraffin, and cut into 5  $\mu$ m thick sections. The sections were processed for deparaffinization and rehydration and then stained with Alcian Blue staining and Safranin O—fast green staining, following the manufacturer's protocol.

Bern score quantification was based on the cartilage tissue quality and was performed as previously published.<sup>33</sup> Briefly, each tissue section was scored from 0 to 3 using three different categories, namely, uniformity and darkness of Safranin O—fast green stain, the distance between cells/amount of matrix accumulated, and cellular morphology. The score from each category of each tissue section was then added up for a maximum score of 9. The scoring was performed blindly by three different experimenters on at least three tissue sections from different tissues representing a middle section of the tissue pellets/ossicles.

**2.12. Western Blotting.** Cells were pelleted and lysed with radioimmunoprecipitation buffer (Sigma-Aldrich) with proteinase inhibitor (Roche) on ice for 30 min. The proteins were separated by sodium dodecyl sulfate polyacrylamide gel electrophoresis and transferred to polyvinylidene fluoride membranes (Millipore, USA). The membranes were blocked with skim milk (5% in Tris-buffered saline and Tween 20 for 1 h and then incubated with the primary antibodies overnight at 4 °C. The bands were then visualized after incubation for 1 h with horseradish peroxidase-conjugated secondary antibodies by chemiluminescence using an electrochemiluminescence detection kit (Amersham, UK). Lamin A/C was the internal control of SOX9, and GAPDH was the internal control of ACAN, COL2A1, and COL10A1.

**2.13. In Vivo Implantation.** All animal experiments described in the present study were reviewed and approved by the Animal Care and Use Committee of Peking University. For the in vivo study, we chose a murine dorsal subcutaneous pocket model to estimate the bone formation of different scaffolds encapsulated with hBMSCs. The cell-loaded microsphere hydrogels were implanted subcutaneously in mice at 2 and 3 weeks of in vitro chondrogenesis induction and 2 weeks of hypertrophic culture, respectively. Male BALB/c nude mice (6–8 weeks old) were separately implanted with different cell-loaded microsphere hydrogels to assess the osteogenic mineralization and vascular recruitment capacity. After mice had been anesthetized by intraperitoneal injection of sodium pentobarbital (70  $\mu$ g g<sup>-1</sup>), two independent incisions were created subcutaneously on the back of each mouse. The mice were euthanized at 4 weeks ( $n = 18$ ) postsurgery, and the samples were excised, photographed, and fixed overnight in 4% paraformaldehyde.

The bone mineral density (BMD) formed in the explants was visualized and quantified using micro-CT. The explants were imaged (60 kV, 0.22 mA, 60 s) using a high-resolution micro-CT specimen scanner (Inveon MM CT; Siemens, Germany). BMD was measured using Inveon Research Workplace software (Siemens). A threshold (1000–4500 mg HA/cc) was determined subjectively from the reconstructed images to partition mineralized tissue from fluid and soft tissues. Afterward, the samples were processed for paraffin sections, and the sections (5  $\mu$ m) were processed for H&E, Safranin O—fast green, and immunofluorescence staining. The primary antibodies for immunofluorescence staining, including COL2A1, COL1A1, RUNX2, OCN, and CD31, were all purchased from Abcam. Quantitative analysis of immunofluorescence staining was analyzed using ImageJ software. Microvessel density was reported as the average number of erythrocyte-filled vessels (vessels mm<sup>-2</sup>) and the average number of vessels per pore using ImageJ software.

**2.14. In Situ Osteochondral Defect Regeneration.** The rabbit BMSCs (rBMSCs; Cyagen, China) were maintained in high glucose DMEM supplemented with 10% fetal bovine serum and 1% penicillin/streptomycin and used at passage 4. rBMSCs were incubated ( $1 \times 10^7$  cells per mL) on different scaffolds, and endochondral ossification was induced in vitro, which was cultured for 3 weeks in chondrogenic

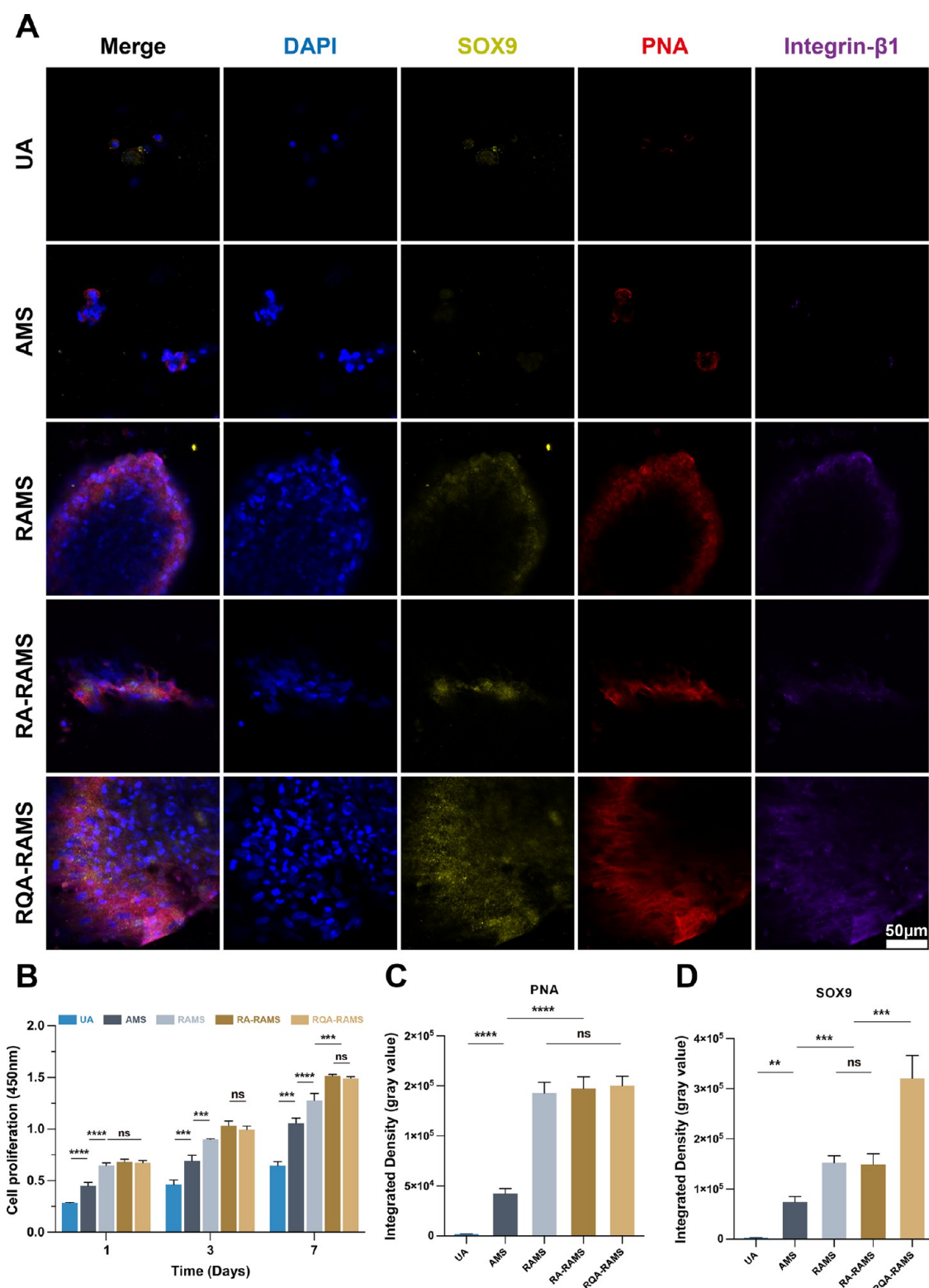


**Figure 2.** Proliferation and aggregation of hBMSCs grown in different groups. (A) Confocal micrographs of hBMSCs after seeding in various scaffolds for 3 days (yellow, labeled with SOX9; red, labeled with PNA; purple, labeled with Integrin  $\beta$ 1 and counterstained with DAPI for nuclei in blue). (B) Proliferation of hBMSCs grown in UA (unmodified alginate hydrogel), AMS (unmodified alginate microscaffolds), RAMS (RGD-peptide-modified alginate microscaffolds), RA-RAMS (RAMS encapsulated in the RGD-peptide-modified alginate hydrogel), and RQA-RAMS (RAMS encapsulated in the RGD- and QK-peptide-comodified alginate hydrogel); scale bar = 50  $\mu$ m. (C) Analysis of PNA and (D) SOX9 expression in the different groups as measured by fluorescent intensity. The  $p$ -value was calculated by Tukey's posthoc test (\*\* $p < 0.01$ , \*\*\* $p < 0.001$ , and \*\*\*\* $p < 0.0001$ ). All data represent mean  $\pm$  SD ( $n = 3$ ).

medium (high glucose DMEM; 100 nM dexamethasone; 50  $\mu$ g mL<sup>-1</sup> ascorbic acid; 50  $\mu$ g mL<sup>-1</sup> L-proline; 100  $\mu$ g mL<sup>-1</sup> sodium pyruvate; 1%

ITS+; 1% P/S; 10 ng mL<sup>-1</sup> TGF- $\beta$ 3; 1 mM CaCl<sub>2</sub>) and 2 weeks in hypertrophic medium (high glucose DMEM; 1 nM dexamethasone; 50

$\mu\text{g mL}^{-1}$  ascorbic acid;  $50 \mu\text{g mL}^{-1}$  L-proline;  $100 \mu\text{g mL}^{-1}$  sodium pyruvate; 1% ITS+; 1% P/S;  $50 \mu\text{g mL}^{-1}$  L-thyroxine; 5 mM  $\beta$ -glycerophosphate; 1 mM  $\text{CaCl}_2$ ).

For the osteochondral defect, the experiments were performed on 10 New Zealand rabbits (male, 2.5–3.0 kg) according to the Ethical Principles of Peking University Institutional Animal Care and Use Committee. After being anesthetized with 3% sodium pentobarbital, the rabbits were shaved and disinfected. The medial parapatellar approach was applied to expose the knee joints. The joints were fully exposed to develop a cylindrical osteochondral defect (4 mm diameter and depth) by a dental drill on both limbs at the center of the groove (Figure S6). The animals were grouped as follows: Normal (normal osteochondral tissue with no treatment), RQA-K@RAMS, Defect (defect alone with no treatment), RQA-K@RAMS-Cell (rBMSCs-laden RQA-K@RAMS without induction in vitro), RQA-K@RAMS-Cell2W (rBMSCs-laden RQA-K@RAMS induced for 2 weeks in vitro), and RQA-K@RAMS-Cell5W (rBMSCs-laden RQA-K@RAMS induced for 5 weeks in vitro). The rabbits were euthanized at 4 weeks postsurgery.

Following animal sacrifice, the knee joint of each rabbit was extracted, photographed, and fixed in neutral formalin (Solarbio) for 3 days. Micro-CT imaging was performed as described above in the subcutaneous study. The bone volume fraction (BV/TV), bone trabeculae number (Tb.N), bone trabecular spacing (Tb.Sp), and bone trabecular thickness (Tb.Th) were measured using Inveon Research Workplace software (Siemens).

For histological analysis, the samples were decalcified in 15% EDTA solution. The decalcification liquid was replaced daily until the sample could be embedded in paraffin. The center of the repair site was sliced into  $5 \mu\text{m}$  sections, followed by H&E staining, Safranin O–fast green, and Movat-Russell Modified Pentachrome Stain staining.

The International Cartilage Repair Society (ICRS) evaluation criteria for osteochondral repair were used for scoring.<sup>34</sup> All scoring was performed by three independent individuals who were blinded to the group assignments. The scoring items included the macroscopic performance and the degree of defect repair.

**2.15. Statistical Analyses.** Statistical analysis of the obtained data was performed using Prism 9 software. All data were tested for normality and homogeneity of variance using a QQ plot and Brown–Forsythe test and expressed as the means  $\pm$  standard deviation of three representative experiments. Comparisons between multiple groups were performed by one-way analysis of variance, followed by Tukey's posthoc testing. Unpaired two-tailed Student's *t* tests were used for comparisons between two groups. No exclusion criteria were applied for all analyses. A value of  $p < 0.05$  was considered to be statistically significant.

### 3. RESULTS AND DISCUSSION

**3.1. Preparation and Characterization of RQA-K@RAMS.** Microscaffolds with small physical dimensions facilitate material exchange with good ability to promote cell growth and can be used as a local delivery platform for drugs.<sup>35,36</sup> By imitating the phenomenon of dewdrops on the surface of lotus leaves, we formed microdroplets by dropping sodium alginate solution on Teflon plates and subjected them to lyophilization and calcium ion cross-linking to obtain sodium alginate microscaffolds in the shape of shallow discs and thin sheets, as shown in Figure 1B. Scanning electron microscopy (SEM) images (Figure 1C,D) revealed the size of the microscaffolds was approximately  $0.8 \pm 1.2 \text{ mm}$ , with the internal pore size being approximately  $50 \mu\text{m}$  with high interconnectivity, which provides access to cellular nutrient exchange and metabolic waste excretion and ample space for cell growth, adhesion, proliferation, and maintenance of cellular differentiation phenotypes.<sup>37</sup> SEM scan of RQA-K@RAMS shows that the microscaffold is surrounded by a layer of hydrogel (Figure 1E,G), which forms a porous structure on the order of microns

( $30 \pm 10 \mu\text{m}$ ) after lyophilization. However, the freeze-dried hydrogels can hardly reflect the actual structure and size of pores in the hydrated state.<sup>38,39</sup> It is worth noting that the internal pore size of the microscaffold is larger than the hydrogel layer in the microscaffold–hydrogel composites, which is critical for developing a local drug release platform.

We examined the ability of the sodium alginate microscaffold–hydrogel composites to release KGN (Figure 1H) by first encapsulating KGN in RQA hydrogel (K-RQA) and found that, because of the nonaffinity of the gel matrix for hydrophobic KGN, approximately 50% of the total amount of KGN was released by day six. This high release rate could not provide an effective controlled release of KGN and was not conducive to providing a continuous environment to induce differentiation in stem cells. We then soaked the microscaffolds in KGN solution for 12 h and lyophilized them to obtain K@RAMS (KGN-laden RGD-peptide-modified alginate microscaffolds). After KGN was physically adsorbed by the microscaffolds, the total amount of KGN released on day six was only approximately 30% of the total amount. Additionally, K@RAMS were mixed with RQA (RQA-K@RAMS) to form a hydrogel layer, and the amount of KGN released during the first 7 days was lower compared with the other two groups, with only 50% of the total amount of KGN released on day 18. The cumulative amount of KGN released in the K@RAMS and RQA-K@RAMS groups increased slowly with the increase of release days, whereas the release curve of the K-RQA group leveled off after 2 weeks. KGN can be optimally adsorbed and persist in the gel matrix through the controlled release effect of the microscaffolds by analyzing the release trend of KGN in different encapsulation systems.

Degradation is an inevitable and objective phenomenon for ionic cross-linked alginate biomaterials.<sup>21</sup> We used the FITC-QK peptide to characterize the degradation of the hydrogel layer on the surface of the microscaffolds (Figure 1I). The FITC-QK peptide was covalently grafted on sodium alginate, which was gradually released with the degradation of the hydrogel layer. Because the added RGD- and QK-peptide-comodified sodium alginate solution was in excess, that which was not in contact with the microscaffolds was free in the solution and accounted for approximately 13.38% of total. The RQA hydrogel layer was formed by cross-linking the residual calcium ions on the surface of the microscaffolds with lower cross-linking strength. The degradation of the RQA hydrogel layer increased with time, with approximately 50% degradation by day nine and continuation until 5 weeks, which indicated that the sodium alginate microscaffold hydrogel composite has the ability to slow-release drugs in stages. The sustained release of QK peptide demonstrates potential beneficial conditions for angiogenesis.

**3.2. RQA-RAMS Promotes the Proliferation and Aggregation of hBMSCs In Vitro.** We investigated the effect of different scaffold types on cell proliferation and aggregation behavior by preparing UA (unmodified alginate hydrogel) and AMS (unmodified alginate microscaffolds) and inoculating them both with hBMSCs. We performed a CCK-8 assay of hBMSCs for 1, 3, and 7 days, and the results suggested that AMS facilitates the promotion of cell proliferation compared with UA (Figure 2B). Ideally, microscaffolds should have interconnected porosity and pores greater than  $20 \mu\text{m}$  to accommodate most types of mammalian cells and allow fluid transfer from the surface to the core of the microscaffold.<sup>40–42</sup> However, cell ingrowth and nutrient transport are also influenced by the dimensions and thickness of porous scaffolds. The large physical dimensions of the currently used porous scaffolds restrict

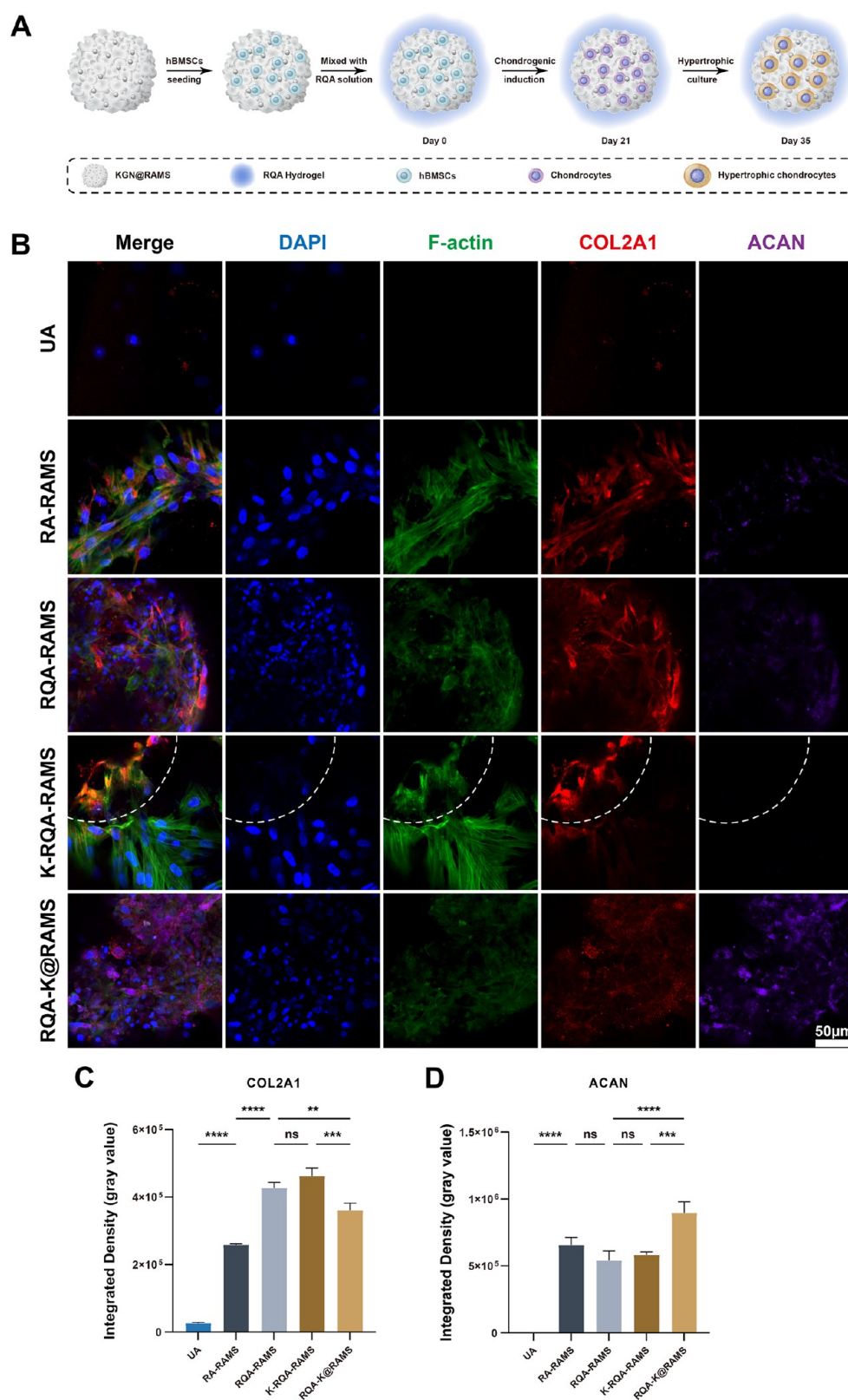


**Figure 3.** Cartilage-related protein expression of hBMSCs grown in different groups by chondrogenic induction for 14 days. (A) Schematic illustration of the induction process of endochondral ossification in vitro. (B) Confocal micrographs of hBMSCs (green, labeled with FITC-phalloidin; red, labeled with COL2A1; purple, labeled with ACAN and counterstained with DAPI for nuclei in blue). The white dashed line represents the junction between the hydrogel layer and the surface of the microscaffolds; scale bar = 50  $\mu\text{m}$ . (C) Analysis of COL2A1 and (D) ACAN expression in the different groups by fluorescent intensity. The  $p$ -value was calculated by Tukey's posthoc test (\*\* $p < 0.01$ , \*\*\* $p < 0.001$ , and \*\*\*\* $p < 0.0001$ ). All data represent mean  $\pm$  SD ( $n = 3$ ). K-RQA-RAMS represents RAMS encapsulated in KGN-laden RGD- and QK-peptide-comodified alginate hydrogel; RQA-K@RAMS represents KGN-laden RAMS encapsulated in RGD- and QK-peptide-comodified alginate hydrogel.

nutrients from accessing the scaffolds and produce undesirable conditions for cell survival and proliferation, which leads to ineffective cell treatment or limited tissue regeneration.<sup>43,44</sup> Wu et al. found that a thinner scaffold favored the proliferation of human-adipose-derived mesenchymal stem cells in the early stage with consistent mean pore size, but scaffold thickness had no significant effect on cell proliferation in long-term cell culture.<sup>45</sup> Here, AMS with small physical dimensions and an interpenetrating porous structure allowed cells to exchange substances directly with the medium, whereas cells encapsulated in hydrogels required nutrients to diffuse from the medium into the hydrogel, which prevented direct contact between cells and the medium and resulted in a lower proliferation rate.<sup>35</sup> RGD peptide provides an adhesion site for cell growth on the scaffold, so the cell proliferation rate of RAMS (RGD-peptide-modified alginate microscaffolds) is significantly higher than that of AMS. Additionally, a layer of hydrogel wrapped on the surface of the microscaffolds had a pronounced promotion effect on cell proliferation, and there was no significant difference between RA-RAMS (RAMS encapsulated in the RGD-peptide-modified alginate hydrogel) and RQA-RAMS (RAMS encapsulated in the RGD- and QK-peptide-comodified alginate hydrogel). We speculate that the hydrogel layer on the surface of the microscaffolds is thin, hence the nutrients can quickly pass through the hydrogel layer to exchange substances with cells, and the hydrogel layer can effectively prevent cell loss caused by the operation process. When cells are mixed directly with the microscaffolds, cells not in contact with the microscaffolds will be directly lost, and the cells on the surface of the microscaffolds are directly subjected to the shear stress generated during the injection process, which causes cell damage.<sup>46</sup> A layer of hydrogel wrapped on the surface of the microscaffolds can help reduce the adverse effects of the above problems on the cells.

The effect of the sodium alginate micro scaffold hydrogel on cells was further visualized by culturing hBMSCs in the scaffold for 3 days, and we visualized the cell survival status in the scaffold by imaging the cytoskeleton and cell–cell interaction-related adhesion factors NCAM1 and N-cadherin. As shown in Figure S1, the cells are scattered in the UA, the cytoskeleton is not fully extended because of the lack of adhesion sites for sodium alginate, and the low expression of NCAM1 and N-cadherin indicates weak intercellular interactions. The cells in the AMS were clustered together in comparison with the UA, which also lacked adhesion sites but had a relatively extended cytoskeleton because of relatively strong intercellular interactions, thereby indicating that the microscaffolds were more conducive to cell survival. In addition, cells adhered to the microscaffolds with a higher expression of NCAM1 and N-cadherin because of RAMS-grafted RGD peptides. The hBMSCs in the RA-RAMS and RQA-RAMS groups not only had a fully extended cytoskeleton but also partially migrated into the hydrogel on the surface of the microscaffolds, which effectively reduced the problem of cell loss on the surface of the microscaffolds.

Cell aggregation behavior can significantly enhance the potential for multidirectional differentiation of hBMSCs.<sup>14,15</sup> After hBMSCs were cultured in the scaffolds for 3 days, we analyzed the cell aggregation markers [PNA, an intercellular adhesion-associated protein (Integrin  $\beta$ 1), and a chondrogenic differentiation marker (SOX9)] by immunofluorescence and evaluated the aggregation behavior of the hBMSCs in each group. As shown in Figure 2A,C,D, hBMSCs showed no significant difference in integrin  $\beta$ 1 expression in AMS and UA, but the expression of PNA and SOX9 was higher in AMS, which

suggests that microscaffolds facilitate cell aggregation behavior. Additionally, the hBMSCs adhered and aggregated extensively to RAMS with a higher expression of PNA and SOX9 compared with AMS, thereby suggesting that sodium alginate microscaffolds grafted with RGD peptides enhanced cell aggregation behavior by providing adhesion sites. The hydrogel layer around the microscaffolds had no significant effect on cell aggregation behavior, and the highest SOX9 expression was observed in the RQA-RAMS group. Together, these results indicate that RQA-RAMS promotes cell adhesion and proliferation through RGD peptides; the microscaffolds recapitulate cell aggregation behavior; and the hydrogel layer avoids cell loss and damage from shear stress, increases the relative density of cells within the microscaffolds hydrogel, and ultimately enhances the chondrogenic differentiation potential of hBMSCs.

**3.3. RQA-K@RAMS Regulate and Accelerate the Endochondral Ossification Behavior of hBMSCs throughout the In Vitro and In Vivo Phase.** We investigated the role of each component of the functionalized alginate micro scaffold–hydrogel composites (RQA-K@RAMS) in the process of cellular endochondral ossification by inoculating cells on different scaffold systems for in vitro endochondral ossification induction, with 3 weeks in chondrogenic medium and 2 weeks in hypertrophic medium.<sup>32,47</sup> We examined the effects of cartilage differentiation and hypertrophy of hBMSCs at 2 and 5 weeks, respectively (Figure 3A). After chondrogenic induction in vitro for 2 weeks, the chondrogenesis of hBMSCs in different scaffolds was significantly different. We used immunofluorescence staining and quantitative analysis of chondrogenesis-related proteins COL2A1 and ACAN (Figure 3B–D) to find that the cartilage matrix secreted by hBMSCs in UA is mostly deposited at the edge of the hydrogel with little deposited inside. This “edge deposition” phenomenon separates the hydrogel carrier from the culture medium, which is not conducive to the exchange of material between the cells in the gel matrix. Previous studies found that RGD peptide can guide human mesenchymal stem cell differentiation into articular or hypertrophic cartilage phenotypes by mechanical stimulation and enhance cartilage-specific gene expression and matrix synthesis.<sup>48,49</sup> Here, the cytoskeleton of hBMSCs was fully extended and intertwined, and cartilage matrix deposition was evident in both RA-RAMS and RQA-RAMS. We saw higher COL2A1 expression in the RQA-RAMS group than in RA-RAMS, but slightly weaker Aggrecan (ACAN) expression than in RA-RAMS, which indicated that the hydrogel layer of RA and RQA had no significant difference on the chondrogenesis. In two groups, K-RQA-RAMS (RAMS encapsulated in KGN-laden RGD- and QK-peptide-comodified alginate hydrogel) and RQA-K@RAMS (KGN-laden RAMS encapsulated in RGD- and QK-peptide-comodified alginate hydrogel), we found that the release of KGN affected the cartilage differentiation of hBMSCs. In the K-RQA-RAMS group, hBMSCs migrated from the surface of the microscaffolds into the hydrogel layer containing KGN and were accompanied by a high expression of COL2A1, but the expression of COL2A1 and ACAN was not significantly different compared with that of RQA-RAMS. However, in the RQA-K@RAMS group, the expression of both COL2A1 and ACAN was increased, with ACAN expression being the highest. In addition, using immunofluorescence 3D imaging of RQA-K@RAMS (Supplementary Movie), we visualized that hBMSCs were uniformly distributed on the surface of the microscaffolds and that there were obvious stromal deposits inside the scaffolds because KGN is loaded in

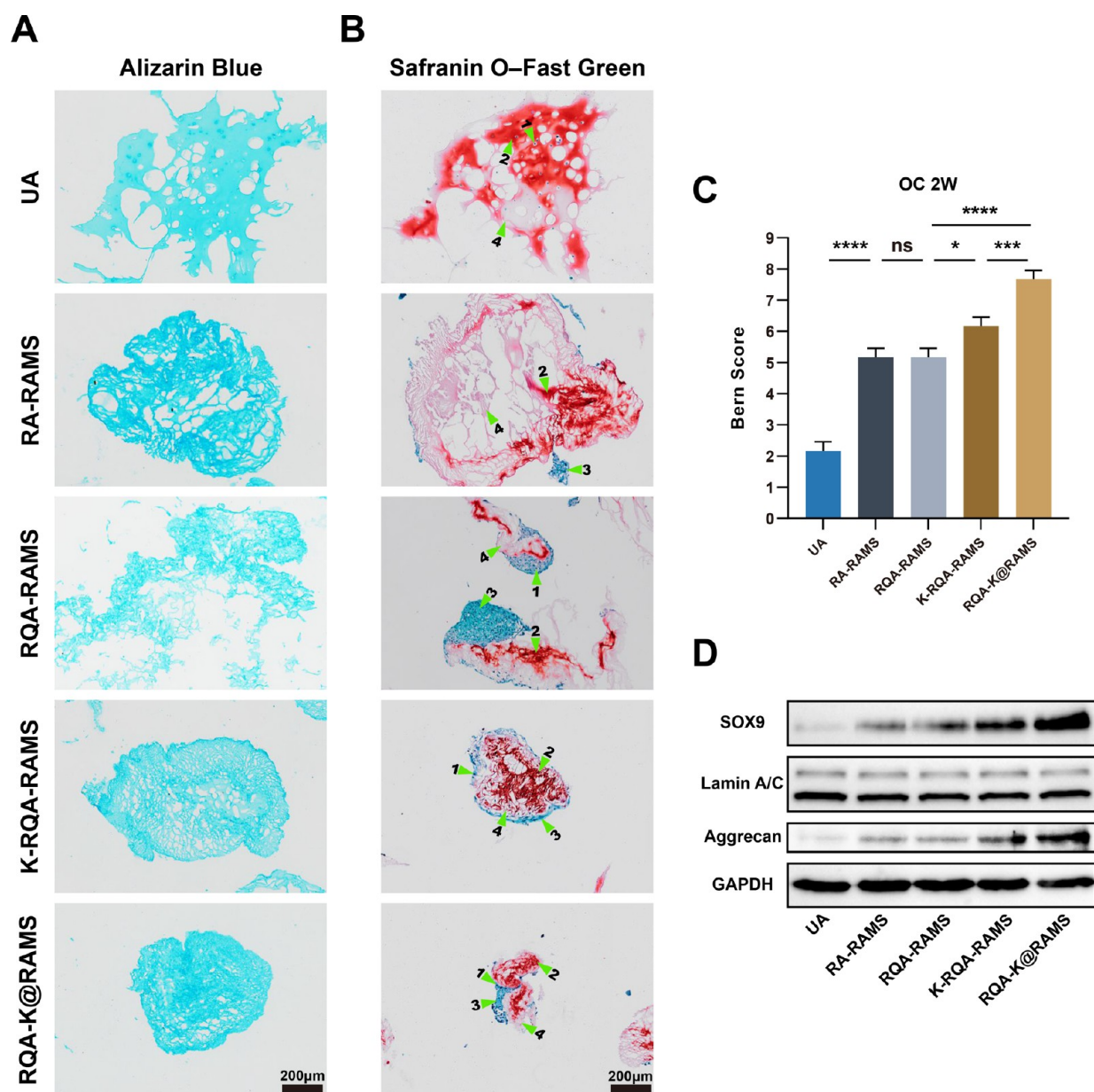


**Figure 4.** Histological staining and Western blot evaluation of cell–scaffold constructs for 2 weeks of in vitro chondrogenesis induction. (A) Alizarin Blue staining (blue represents neo-cartilage matrix). (B) Safranin O–fast green staining (1, chondrocytes; 2, neo-cartilage matrix; 3, collagen fiber; 4, residual sodium alginate materials). (C) Bern scoring for neo-cartilage assessment; OC 2W, chondrogenesis induction 2 weeks in vitro. (D) Western blot analyses of SOX9 and ACAN expression in hBMSCs at 2 weeks. Scale bar = 200  $\mu\text{m}$ . The  $p$ -value was calculated by Tukey's posthoc test (\*\* $p < 0.01$ , \*\*\* $p < 0.001$ , and \*\*\*\* $p < 0.0001$ ). All data represent mean  $\pm$  SD ( $n = 3$ ).

the microscaffolds and needs to pass through the microscaffolds and hydrogel layer sequentially before it can be released into the culture medium, thus achieving a controlled release of KGN and providing a continuous and stable induction microenvironment for the chondrogenic differentiation of hBMSCs.

We observed the tissue composition and internal structure of the cell–scaffold constructs by performing Alizarin Blue and Safranin O–fast green staining and Bern Score evaluation. As shown in Figure 4A,B, hBMSCs were encapsulated in the UA and dispersed from each other; we observed light red staining in the cartilage matrix distributed at the edges of the hydrogel. For the sodium alginate microscaffold–hydrogel, we could observe interconnected pore structures inside the scaffold; most cells adhered and aggregated on the scaffold surface and in the hydrogel layer accompanied by few cells migrating into the

scaffold, and the neo-cartilage matrix was mostly deposited inside the scaffold containing mucin, GAGs, and collagen fibers, thereby indicating that the neo-cartilage components were comprehensive and approaching normal hyaline cartilage tissue. Moreover, we could also clearly observe the aggregation of cells on the surface of the scaffold, with the expression of gray-green collagen fibers between the cells. Measuring the quality of neo-cartilage tissues in each group using the Bern Score (Figure 4C), we found that the neo-cartilage quality of K-RQA-RAMS and RQA-K@RAMS was higher than that of RA-RAMS and RQA-RAMS after KGN loading, with RQA-K@RAMS being the best with darker staining, more intercellular matrix secretion, and mostly round cells with less nuclear consolidation and necrosis. Western blotting of the SOX9 and COL2A1 proteins in the hBMSCs exhibited clear bands after culturing for 2 weeks

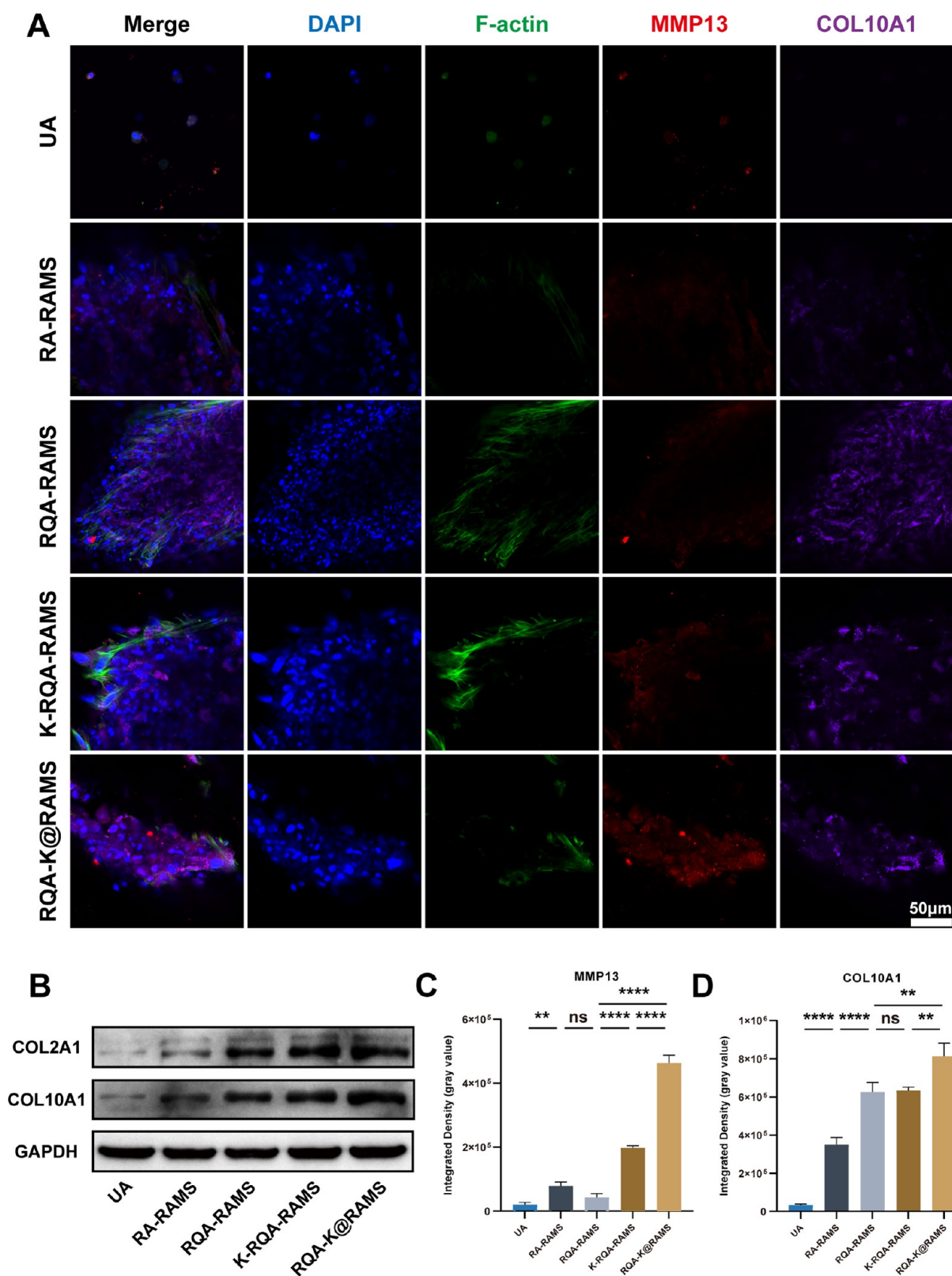


**Figure 5.** Hypertrophic cartilage-related protein expression of hBMSCs grown in different groups by chondrogenic induction at 3 weeks and hypertrophic culture at 2 weeks in vitro. (A) Confocal micrographs of hBMSCs (green, labeled with FITC-phalloidin; red, labeled with MMP13; purple, labeled with COL10A1 and counterstained with DAPI for nuclei in blue); scale bar = 50  $\mu$ m. (B) Western blot analyses of COL2A1 and COL10A1 expression in hBMSCs at 5 weeks. (C) Analysis of MMP13 and (D) COL10A1 expression in the different groups by fluorescent intensity. The *p*-value was calculated by Tukey's posthoc test (\*\**p* < 0.01, \*\*\**p* < 0.001, and \*\*\*\**p* < 0.0001). All data represent mean  $\pm$  SD (*n* = 3).

(Figure 4D). Chondrocytes express a characteristic genetic program driven by SOX9.<sup>50</sup> We could observe that SOX9

expression was not significantly different between RA-RAMS and RQA-RAMS, but higher than in the UA group; the two

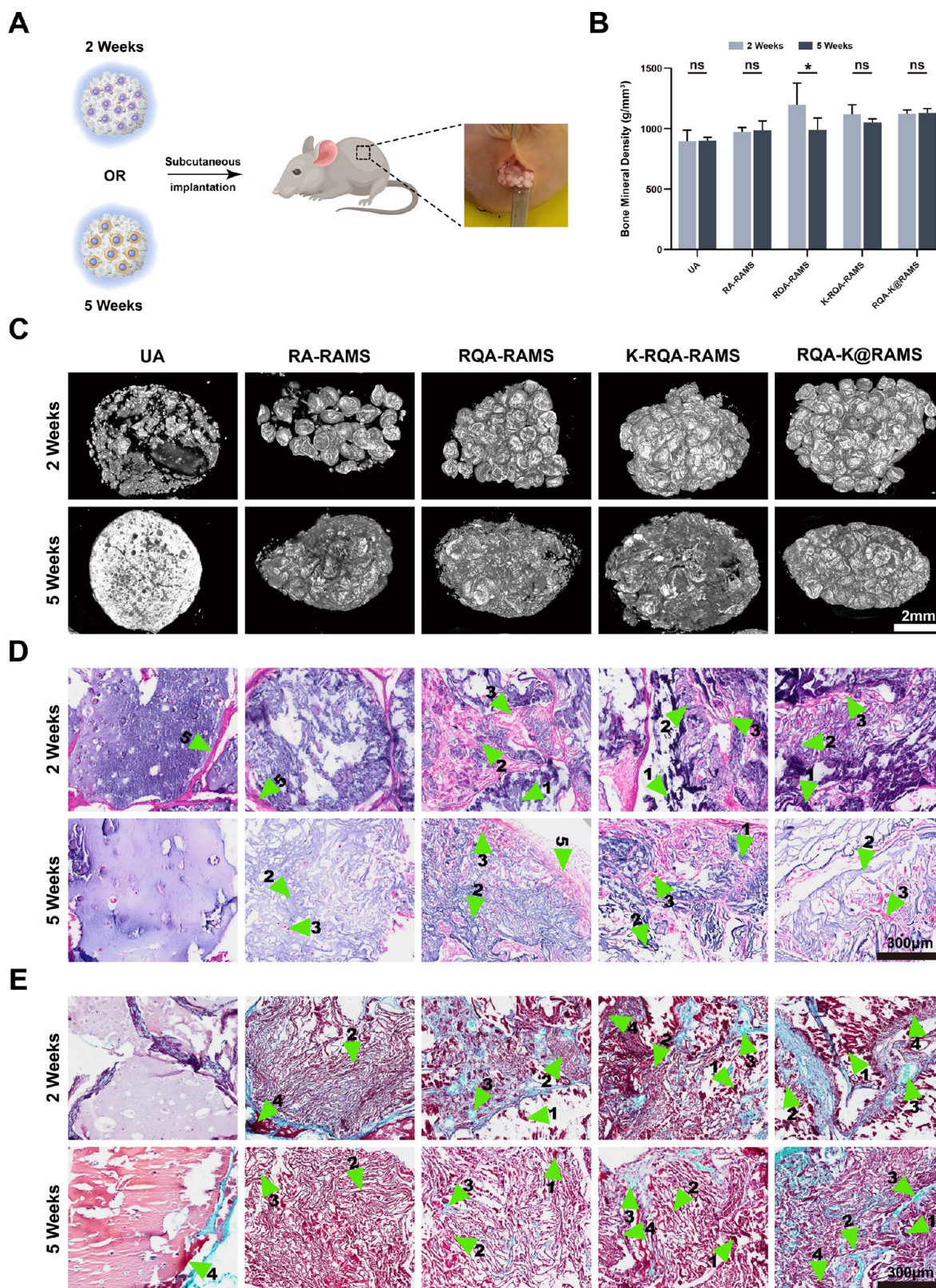


**Figure 6.** Micro-CT and histological staining of samples taken after 4 weeks of subcutaneous implantation. (A) Schematic illustration of subcutaneous transplantation in nude mice. (B) Quantitative analysis of BMD of different hBMSCs-loaded scaffolds. (C) Micro-CT reconstruction images of hBMSCs mineralization. Scale bar = 2 mm. (D) H&E and (E) Safranin O–fast green staining of the hBMSCs-loaded scaffolds (1, residual sodium alginate hydrogel fragments; 2, residual sodium alginate microscaffolds; 3, new blood vessels; 4, neo-cartilage; 5, implant–host boundary). Scale bar = 300  $\mu\text{m}$ . The  $p$ -value was calculated by unpaired two-tailed Student's  $t$  tests ( $*p < 0.05$ ). All data represent mean  $\pm$  SD ( $n = 3$ ). The label 2 weeks represents in vitro cartilage induction for 2 weeks; 5 weeks represents in vitro cartilage induction for 3 weeks, hypertrophy for 2 weeks.

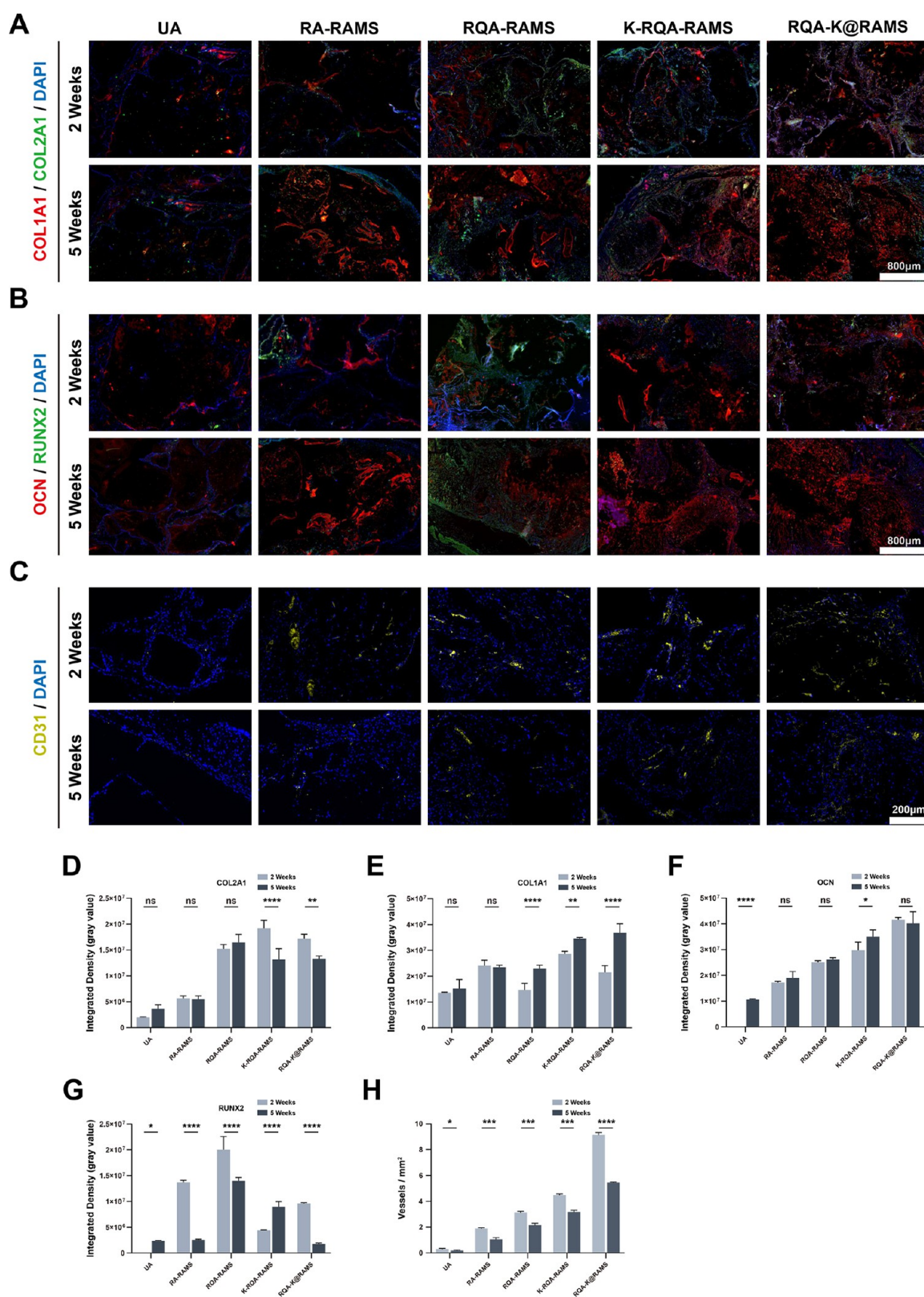


**Figure 7.** Expression of endochondral ossification-related proteins and vascularization after 4 weeks of subcutaneous implantation samples. (A,B) Immunofluorescence staining to detect COL1A1, COL2A1, RUNX2, and OCN (green = COL2A1, RUNX2; red = COL1A1, OCN; blue = cell nuclei). Scale bar = 800  $\mu\text{m}$ . (C) Immunofluorescence staining of CD31 (yellow, CD31; blue, cell nuclei). Scale bar = 200  $\mu\text{m}$ . (D) Analysis of COL2A1, (E) COL1A1, (G) RUNX2, and (F) OCN expression in the different groups by fluorescence intensity. (H) Analysis of total perfused microvessel density (CD31). The  $p$ -value was calculated by unpaired two-tailed Student's  $t$  tests ( $*p < 0.05$ ,  $**p < 0.001$ , and  $****p < 0.0001$ ). All data represent means  $\pm$  SD ( $n = 3$ ).

groups K-RQA-RAMS and RQA-K@RAMS of loaded KGN had more remarkable SOX9 expression, with RQA-K@RAMS showing the strongest expression. Aggrecan (ACAN), a chondroitin/keratan sulfate-containing proteoglycan, is a major component of cartilaginous tissues.<sup>51</sup> We found that the expression trend of ACAN was consistent with that of SOX9, and hBMSCs had the highest expression of ACAN in RQA-K@RAMS, which indicated that RQA-K@RAMS, with the controlled release of KGN, is more conducive to the differentiation of hBMSCs toward chondrocytes, accompanied by a large amount of cartilage matrix secretion.

The cartilage matrix secretion in different cell–scaffold constructs was changed after 3 weeks of chondrogenic induction and 2 weeks of hypertrophic culture, as observed by immunofluorescence analysis (Figure S2). From 2 to 5 weeks, the expression of ACAN decreased, and COL2A1 increased in the K-RQA-RAMS and RQA-K@RAMS groups. No significant difference was observed in the RA-RAMS and RQA-RAMS groups, which still had significantly higher expressions than in the UA group; there was a relative decrease in COL2A1 in RQA-RAMS compared with RA-RAMS. The K-RQA-RAMS group had the highest secretion of COL2A1, whereas the RQA-K@RAMS group had the highest secretion of ACAN, and the difference was more pronounced at 2 weeks compared with the other four groups. We used histological staining (Figure S3A) and found that hBMSCs showed partial degradation of the internal pore structure of the microscaffolds and deposition of red-stained cartilage matrix inside the scaffolds after 5 weeks of induction in different scaffold systems in vitro, which was similar to at 2 weeks. We used Bern score to evaluate the quality of cartilage tissue at 5 weeks (Figure S3B) and found that the neo-cartilage decreased at 5 weeks of in vitro induction when compared with 2 weeks, but the trend did not change significantly between the groups. The neo-cartilage quality was highest in the RQA-K@RAMS group and not significantly different in the RA-RAMS and RQA-RAMS groups, which were lower than the K-RQA-RAMS group but higher than the UA group.

We examined the formation of hypertrophic cartilage by performing immunofluorescence and Western blot assays of the cell–scaffold constructs at 5 weeks (Figure 5). Previous studies found that the expression of COL10A1 was up-regulated after RGD-modified scaffolds were cultured in vitro; sodium alginate hydrogel with fast stress relaxation behavior can significantly promote chondrocyte proliferation and volume increase.<sup>22,23,52</sup> Here, we found that RA-RAMS (sodium alginate micro-scaffold–hydrogel grafted with RGD peptides) exhibited a stronger expression of COL10A1 and MMP13 than in the UA group. However, the expression of COL10A1 was higher in the RQA-RAMS group than in the RA-RAMS group, which indicated that more COL10A1 was present in the cartilage matrix formed in the RQA-RAMS group. Because QK peptide is a mimetic peptide of VEGF, whether QK peptide, as well as RGD peptide and QK peptide modified in a 1:1 ratio, are beneficial for chondrocyte hypertrophy needs further investigation. The expression of COL10A1 and MMP13 was higher in both the K-RQA-RAMS and RQA-K@RAMS groups than in the RA-RAMS and RQA-RAMS groups, mainly because the K-RQA-RAMS and RQA-K@RAMS groups induced better chondrogenic differentiation of hBMSCs and more chondrogenic matrix secretion compared with the RA-RAMS and RQA-RAMS groups, which in turn exhibited more significant chondrocyte hypertrophy. The Western blot assay showed the

highest expression of COL2A1 and COL10A1 in the RQA-K@RAMS group, thereby indicating that the strategy of sequential induction of differentiation could better promote chondrocyte hypertrophy by enhancing the chondrogenic differentiation of hBMSCs. Surprisingly, the cell–scaffold constructs after 2 weeks of in vitro cartilage induction also showed expression of the hypertrophic cartilage markers COL10A1 and MMP13 (Figure S4).

Hypertrophic chondrocytes express COL10A1 in the early and middle stages and MMP13 in the late stages; existing studies suggest that the quality of endochondral ossification in vivo is related to the maturation of hypertrophic cartilage.<sup>32,53,54</sup> We hypothesize that functionalized sodium alginate micro-scaffold–hydrogel accelerates endochondral ossification by regulating the endochondral ossification behavior of hBMSCs throughout the whole process. However, in vivo experiments are needed to demonstrate that the accelerated endochondral ossification process does not affect osteogenic mineralization and vascular recruitment effects. Therefore, we performed subcutaneous ectopic osteogenesis experiments in nude mice with cell–scaffold constructs at two time points: 2 weeks (in vitro cartilage induction for 2 weeks) and 5 weeks (in vitro cartilage induction for 3 weeks, hypertrophy for 2 weeks), respectively, and removed the samples after 4 weeks of implantation in vivo to explore the differences in their osteomineralization capacity and vascularization (Figure 6A).

Through micro-CT morphology and analysis of bone mineralization (Figure 6B,C), we found that the surface of the samples induced in vitro for 5 weeks in the UA group was completely surrounded by the bone matrix, which was not conducive to material exchange and vascular migration of the cells in the hydrogel matrix. The shape of the microscaffolds was clearly visible in the samples induced in vitro for 2 weeks compared with those induced in vitro for 5 weeks, whereas the shape of the microscaffolds was blurred in the 5 weeks samples because of the degradation of the microscaffolds. Analysis of bone mineral density (BMD) in the subcutaneous samples showed no significant difference in BMD between hBMSCs in the constructed functionalized sodium alginate micro-scaffold–hydrogel system at 2 weeks and 5 weeks induction in vitro. Additionally, we observed partial degradation of the scaffold structure inside the samples by H&E and Safranin O–fast green staining (Figure 6D,E), as well as obvious matrix deposition and vascular growth into the samples. Clear luminal structures and scattered red blood cells could be noticed, which indicated that the cell–scaffold complex facilitated the migration of blood vessels.

Furthermore, we used immunofluorescence to detect the expression of endochondral ossification-related proteins in the samples (Figure 7A,B,D,F) and found that COL2A1, COL1A1, RUNX2, and OCN were expressed in the bone matrix formed by all groups. The samples with 2 weeks had more COL2A1 expression, whereas the samples with 5 weeks had more significant COL1A1 expression. At 2 weeks of in vitro cartilage induction, all three groups, RQA-RAMS, K-RQA-RAMS, and RQA-K@RAMS, had higher COL2A1 expression and were superior to the RA-RAMS and UA groups, whereas COL1A1 expression differed little between the groups and was relatively higher in the RA-RAMS and K-RQA-RAMS groups. With 3 weeks of in vitro cartilage induction and 2 weeks of hypertrophy, COL2A1 levels were relatively high in the RQA-RAMS group, and COL2A1 expression was not significantly different in the K-RQA-RAMS and RQA-K@RAMS groups but was higher than in

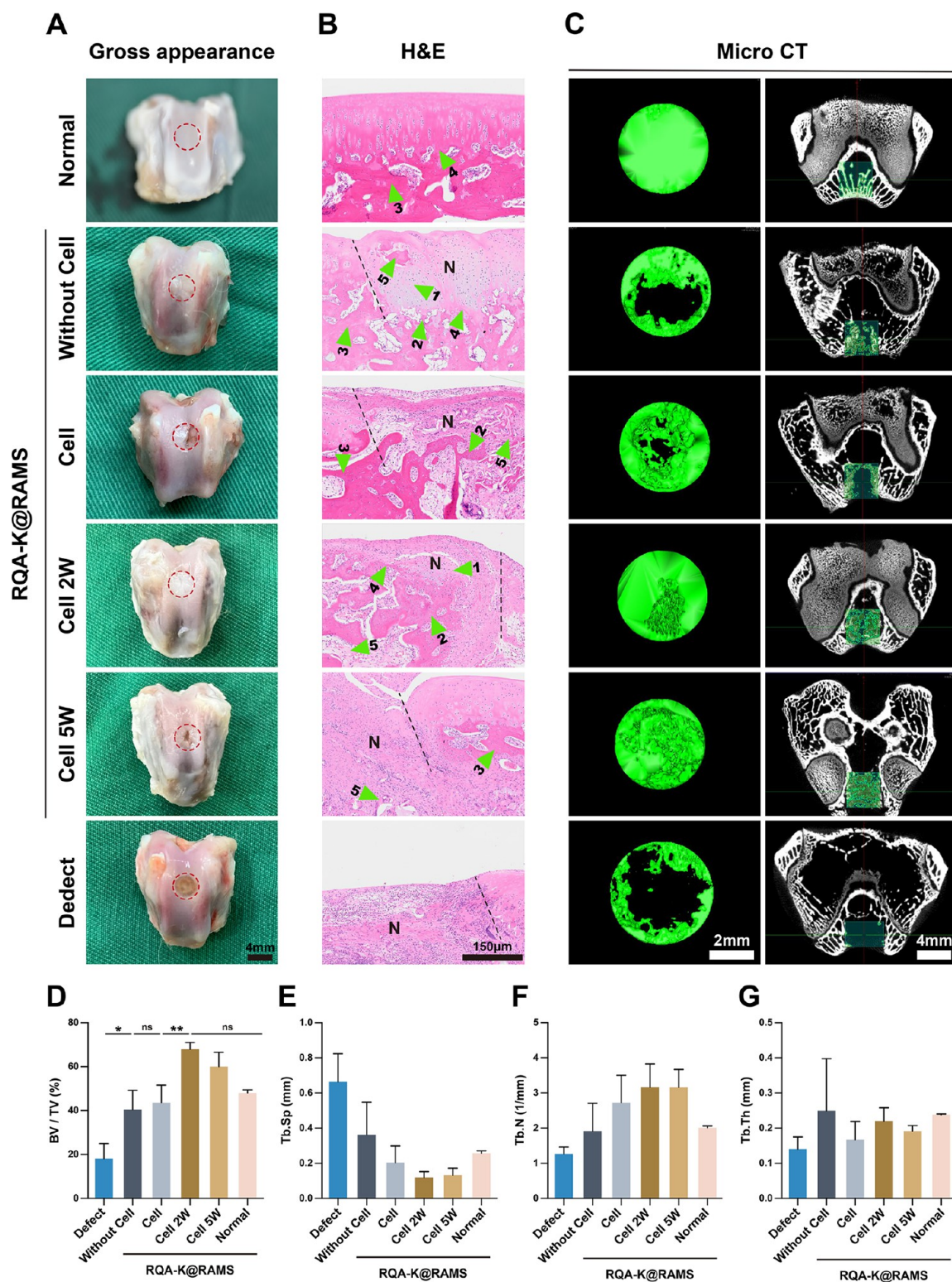


**Figure 8.** In situ osteochondral tissue regeneration by different groups. (A) Macroscopic results for bone defects after 4 weeks; the red dotted circle represents the location of the defect. Scale bar = 4 mm. (B) H&E staining of defective superficial cartilage repair (1, neo-cartilage; 2, new bone trabeculae; 3, normal bone trabeculae; 4, cartilage and subchondral bone borders; 5, residual sodium alginate materials). The black dashed line represents the junction between the cartilage defect and the new tissue; N represents the formation of new tissues; scale bar = 300  $\mu$ m. (C) Representative micro-CT images and (D–G) quantitative histomorphometry analyses of bone regeneration in osteochondral defects (BV/TV, the bone volume fraction; Tb.Sp, the bone trabecular separation; Tb.N, the bone trabecular number; Tb.Th, the bone trabecular thickness). Left scale bar = 2 mm; right scale bar = 4 mm. “Normal” represents normal osteochondral tissue; “Defect” represents defect alone with no treatment; “RQA-K@RAMS-Cell” represents rBMSCs-laden RQA-K@RAMS without induction in vitro; “RQA-K@RAMS-Cell2W” represents rBMSCs-laden RQA-K@RAMS induced for 2 weeks in vitro; “RQA-K@RAMS-Cell5W” represents rBMSCs-laden RQA-K@RAMS induced for 5 weeks in vitro. The *p*-value was calculated by Tukey’s posthoc test (\**p* < 0.05 and \*\**p* < 0.01). All data represent mean  $\pm$  SD (*n* = 3).

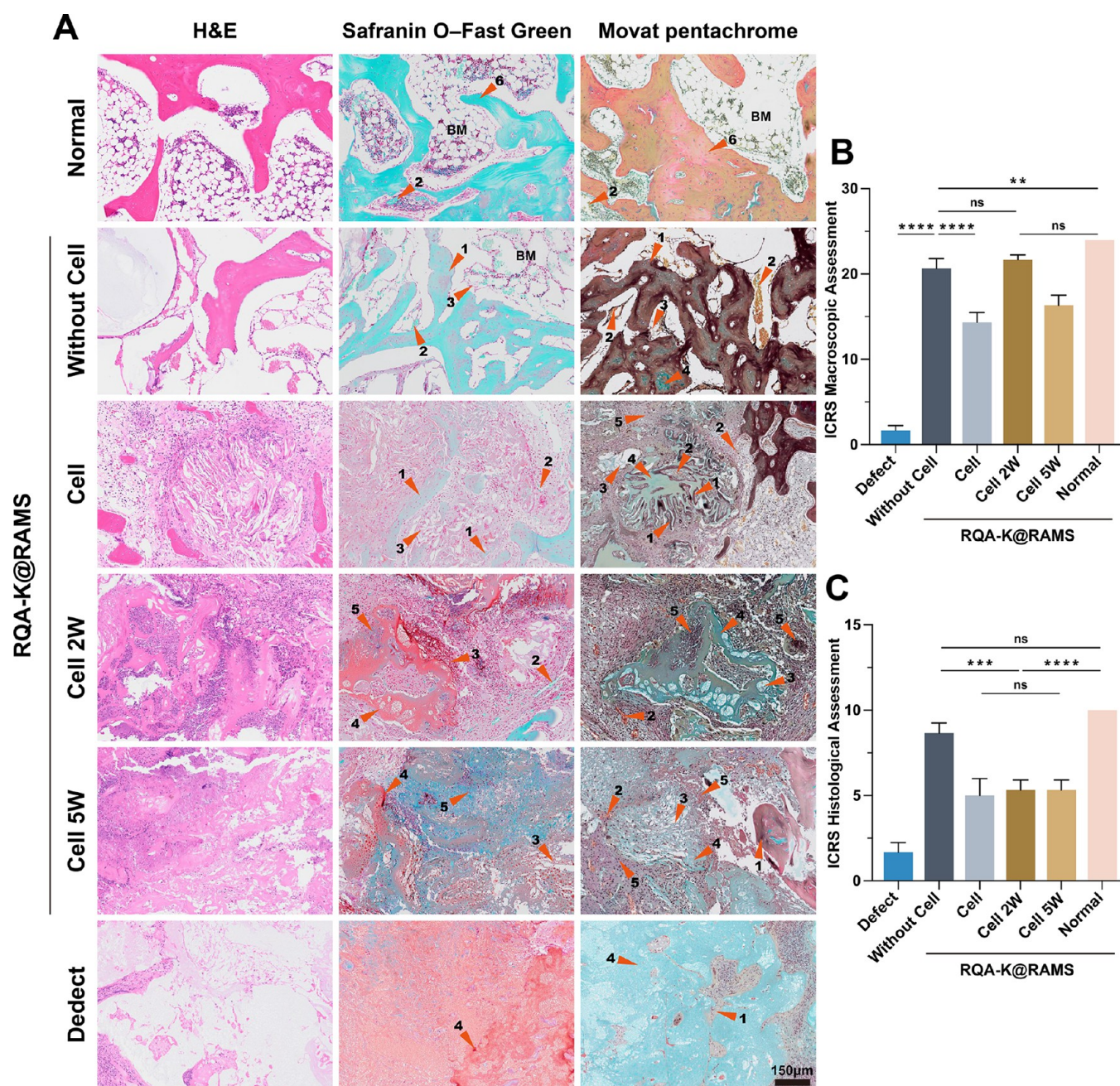


**Figure 9.** Histological staining and osteochondral repair evaluation of the implantation samples in osteochondral defects after 4 weeks. (A) H&E, Safranin O–fast green, and Movat pentachrome staining in each group at 4 weeks postsurgery (1, new bone trabeculae; 2, new blood vessels; 3, residual material; 4, neo-cartilage; 5, mineralized bone matrix deposits; 6, normal bone trabeculae; BM, bone marrow). Scale bar = 150  $\mu$ m. (B) ICRS evaluation for macroscopic performance and (C) the degree of defect repair. The  $p$ -value was calculated by Tukey's posthoc test (\*\* $p < 0.01$ , \*\*\* $p < 0.001$ , and \*\*\*\* $p < 0.0001$ ). All data represent mean  $\pm$  SD ( $n = 3$ ). "Normal" represents normal osteochondral tissue; "Defect" represents defect alone with no treatment; "RQA-K@RAMS-Cell" represents rBMSCs-laden RQA-K@RAMS without induction in vitro; "RQA-K@RAMS-Cell2W" represents rBMSCs-laden RQA-K@RAMS induced for 2 weeks in vitro; "RQA-K@RAMS-Cell5W" represents rBMSCs-laden RQA-K@RAMS induced for 5 weeks in vitro.

the RA-RAMS and UA groups. RUNX2 is essential for transdifferentiation and is required for maintaining the survival of hypertrophic chondrocytes.<sup>55</sup> The samples in 2 weeks had more RUNX2 expression than 5 weeks, thereby indicating that the samples in 2 weeks were in the stage of transformation of hypertrophic chondrocytes to osteoblasts. OCN is a marker of osteoblasts, whose high expression represents mineralization and maturation of the bone matrix.<sup>56</sup> The RQA-K@RAMS group showed the highest OCN expression at both 2 and 5

weeks, which indicated that the functionalized sodium alginate microsphere–hydrogel composites contributed to the rapid transformation and mineralization of hypertrophic chondrocytes to osteoblasts in vivo, and there was no significant difference in the osteogenic ability of the hBMSCs at 2 and 5 weeks of induction in vitro. During endochondral ossification, invading vasculature can activate the expression of the core pluripotency genes in hypertrophic chondrocytes to promote osteogenic transformation.<sup>25</sup> Digital images of subcutaneously

implanted 4 week samples (Figure S5) and CD31 staining (Figure 7C,H) results suggest that RQA-K@RAMS contributes to the establishment of a vascularized microenvironment in vivo. The UA group had almost no migration of vascular endothelial cells because its surface was covered with dense bone matrix; the three groups of RQA-RAMS, K-RQA-RAMS, and RQA-K@RAMS grafted with QK peptide had more migration of vascular endothelial cells to the inside of the scaffold compared with RA-RAMS not grafted with QK peptide, and obvious wall structures could be seen with the largest area of neovascularization in RQA-K@RAMS. These results confirmed that functionalized sodium alginate microsphere–hydrogel composites significantly accelerate the endochondral ossification process by regulating cellular endochondral ossification behavior and that they exhibit good osteogenic mineralization and vascular recruitment after implantation.

**3.4. In Situ Osteochondral Tissue Regeneration by RQA-K@RAMS.** In situ osteochondral tissue regeneration is critical for future clinical translational applications of RQA-K@RAMS. In this study, various specimens were implanted into the osteochondral defects of the rabbit knee joint, and the new tissue formation and development were evaluated at 4 weeks postsurgery. Gross appearance (Figure 8A) and micro-CT images (Figure 8C) of the osteochondral defects in different groups show that all groups had neo-cartilage formation in the area of cartilage defects. The cartilage matrices formed in the RQA-K@RAMS and RQA-K@RAMS-Cell2W group (rBMSCs-laden RQA-K@RAMS induced for 2 weeks in vitro) were smooth and completely covered the bone defect, whereas the cartilage matrices formed in the RQA-K@RAMS-Cell group (rBMSCs-laden RQA-K@RAMS without induction in vitro), RQA-K@RAMS-Cell5W group (rBMSCs-laden RQA-K@RAMS induced for 5 weeks in vitro), and Defect group (defect alone with no treatment) were rough and had an obvious granular surface, which increased friction during joint movement and was not conducive to the functional reconstruction of the joint. H&E staining (Figure 8B) of the samples also confirmed that the cartilage layer formed at the osteochondral defect in the FA group was clearly delineated from the subchondral bone layer, exhibited bean-shaped chondrocyte morphologies with canonical pericellular matrices, and was thicker than the surrounding cartilage layer.<sup>57</sup> Micro-CT quantitative analysis (Figure 8D–G) showed that the bone volume fraction (BV/TV) was higher in the RQA-K@RAMS-Cell2W and RQA-K@RAMS-Cell5W groups than in normal osteochondral tissue, whereas the BV/TV levels in the RQA-K@RAMS (without cell) group were similar to those of normal osteochondral tissue. BV/TV reflects the amount of new bone formation in each group. Both the RQA-K@RAMS-Cell2W and RQA-K@RAMS-Cell5W groups underwent induction of endochondral ossification in vitro with enriched cartilage matrix, so the BV/TV reached an impressive 67.9% and 60.0%, respectively. Moreover, three indicators of the number, thickness, and dispersion of the new bone trabeculae indicated that the spacing of the trabeculae was the smallest in the RQA-K@RAMS-Cell2W and RQA-K@RAMS-Cell5W groups because they were inherently rich in cartilage matrix, whereas the parameters of the new bone trabeculae were not significantly different through the RQA-K@RAMS and RQA-K@RAMS-Cell groups, which were similar to normal osteochondral tissue. Although the RQA-K@RAMS-Cell2W and RQA-K@RAMS-Cell5W groups had the best new bone formation parameters, better than normal osteochondral tissue, they failed to form a

sparse irregular meshwork with similar parameters to normal bone trabeculae and could not provide cushioning protection when subjected to joint stress.

We analyzed the histological structure and composition of the osteogenic region by performing histological staining (Figure 9A), which showed that the RQA-K@RAMS-Cell, RQA-K@RAMS-Cell2W, and RQA-K@RAMS-Cell5W groups had a large deposit of mineralized bone matrix surrounded by blood vessels in the bone defect and cartilage matrix within the undegraded material, but the overall structure was relatively disorganized and new bone trabeculae were rare. Recently, Sébastien constructed devitalized human hypertrophic cartilage, a cell-free material that induces bone formation by apoptosis-driven devitalization and lyophilization, which exhibits unprecedented osteoinductive properties.<sup>58</sup> We, therefore, suspect that the immunogenicity of hypertrophic cartilage grafts formed by endochondral ossification of exogenous cells makes it difficult to integrate effectively with the host at the implanted bone defect, thereby resulting in a poorly coordinated endogenous tissue regeneration response. Moreover, the rBMSCs used in the RQA-K@RAMS-Cell2W and RQA-K@RAMS-Cell5W groups must be amplified extensively in vitro, and the increase in the number of passages can affect the proliferation and differentiation of MSCs, which in turn affects the osteogenic repair effect.<sup>59–62</sup> Notably, a denser trabecular structure was formed in the RQA-K@RAMS group, surrounded by partially undegraded material; a blue-stained cartilage matrix was visible inside the new trabeculae; and blood vessels were enriched around the new trabeculae, thereby providing nutrients and oxygen to facilitate endochondral ossification. The International Cartilage Repair Society (ICRS) score (Figure 9B,C) also demonstrated that the new osteochondral tissue in the RQA-K@RAMS group was close to normal osteochondral tissue.

## 4. CONCLUSIONS

Endochondral ossification is regulated by a complex and lengthy sequence of cellular behaviors. In this study, a functionalized sodium alginate microsphere–hydrogel composite was designed to accelerate osteochondral repair via sequentially modulating cellular ECO behavior. RGD-peptide-modified microscaffolds can recapitulate cell proliferation and aggregation behavior and facilitate material exchange between cells and the external environment because of their large specific surface area and 3D porous structure. Sodium alginate microsphere–hydrogel composites provide a continuous and stable chondrogenic induction microenvironment for the chondrogenic differentiation of hBMSCs through the slow release of KGN, while the formation of more chondrocytes further promotes chondrocyte hypertrophy. A functionalized sodium alginate hydrogel grafted with RGD and QK peptides helps avoid cell loss from the microscaffolds and cell damage because of shear stress during injection, while RGD peptide facilitates chondrocyte proliferation and hypertrophy, and QK peptide creates a vascular niche conducive to the transformation of hypertrophic chondrocytes into osteoblasts by recruiting vascular endothelial cells to migrate in vivo. In vitro cellular assays demonstrated that RQA-K@RAMS could initially mimic and regulate the whole process of endochondral ossification in hBMSCs. Subcutaneous ectopic osteogenesis in nude mice suggested that RQA-K@RAMS could accelerate endochondral ossification and showed good osteomineralization and vascular recruitment after 2 weeks of in vitro chondrogenesis induction. Moreover, RQA-K@RAMS mediated the bilayer repair of osteochondral defects to

form a smooth cartilage matrix on the surface of the bone defect and dense bone trabeculae with vascular growth inside the bone defect. These results confirmed that functionalized sodium alginate micro scaffold–hydrogel composites have great application potential in osteochondral repair through recapitulating endochondral ossification.

## ■ ASSOCIATED CONTENT

### SI Supporting Information

The Supporting Information is available free of charge at <https://pubs.acs.org/doi/10.1021/acsami.2c12694>.

Morphology of hBMSCs grown in different groups by confocal micrographs; cartilage-related protein expression of hBMSCs grown in different groups by chondrogenic induction for 35 days; histological staining and evaluation of cell–scaffold constructs for 5 weeks of in vitro induction; hypertrophic cartilage-related protein expression of hBMSCs grown in different groups by chondrogenic induction for 14 days; macroscopic results for subcutaneous transplantation in nude mice after 4 weeks; and intraoperative picture of osteochondral defect at the rabbit knee joint (PDF)

Immunofluorescence 3D imaging of RQA-K@RAMS (MP4)

## ■ AUTHOR INFORMATION

### Corresponding Authors

**Lei Zhang** – Central Laboratory and Department of Oral and Maxillofacial Surgery, School and Hospital of Stomatology, Peking University, Beijing 100081, P.R. China; Email: [zhlei\\_doctor@sina.com](mailto:zhlei_doctor@sina.com)

**Shicheng Wei** – Central Laboratory and Department of Oral and Maxillofacial Surgery, School and Hospital of Stomatology, Peking University, Beijing 100081, P.R. China; Laboratory of Biomaterials and Regenerative Medicine, Academy for Advanced Interdisciplinary Studies, Peking University, Beijing 100871, P.R. China; [orcid.org/0000-0001-6024-9615](https://orcid.org/0000-0001-6024-9615); Email: [sc-wei@pku.edu.cn](mailto:sc-wei@pku.edu.cn)

### Authors

**He Zhang** – Central Laboratory and Department of Oral and Maxillofacial Surgery, School and Hospital of Stomatology, Peking University, Beijing 100081, P.R. China

**Qian Li** – Laboratory of Biomaterials and Regenerative Medicine, Academy for Advanced Interdisciplinary Studies, Peking University, Beijing 100871, P.R. China

**Xiangliang Xu** – Central Laboratory and Department of Oral and Maxillofacial Surgery, School and Hospital of Stomatology, Peking University, Beijing 100081, P.R. China

**Siqi Zhang** – Laboratory of Biomaterials and Regenerative Medicine, Academy for Advanced Interdisciplinary Studies, Peking University, Beijing 100871, P.R. China

**Yang Chen** – Laboratory of Biomaterials and Regenerative Medicine, Academy for Advanced Interdisciplinary Studies, Peking University, Beijing 100871, P.R. China

**Tao Yuan** – Key Laboratory of Carcinogenesis and Translational Research (Ministry of Education), Department of Tumor Biology, Peking University Cancer Hospital and Institute, Beijing 100142, P.R. China

**Ziqian Zeng** – Central Laboratory and Department of Oral and Maxillofacial Surgery, School and Hospital of Stomatology, Peking University, Beijing 100081, P.R. China

**Yifei Zhang** – Central Laboratory and Department of Oral and Maxillofacial Surgery, School and Hospital of Stomatology, Peking University, Beijing 100081, P.R. China

**Zi Mei** – Central Laboratory and Department of Oral and Maxillofacial Surgery, School and Hospital of Stomatology, Peking University, Beijing 100081, P.R. China

**Shuang Yan** – Central Laboratory and Department of Oral and Maxillofacial Surgery, School and Hospital of Stomatology, Peking University, Beijing 100081, P.R. China

Complete contact information is available at <https://pubs.acs.org/doi/10.1021/acsami.2c12694>

### Author Contributions

S.W. and L.Z. conceived this project and supervised all experiments. H.Z., Q.L., X.X., S.Z., Y.C., T.Y., Z.Z., Y.Z., Z.M., and S.Y. designed and performed the experiments. H.Z. analyzed the data and drafted the manuscript. S.W. reviewed and made significant revisions to the manuscript. All authors read and approved the final manuscript.

### Notes

The authors declare no competing financial interest.

## ■ ACKNOWLEDGMENTS

All animal procedures were performed in accordance with the regulations approved by the Institutional Animal Care and Use Committee (IACUC) of Peking University. This work was supported by the National Key Research and Development Program of China (2016YFC1102104) and by the Discipline Development Fund of School and Hospital of Stomatology, Peking University. We thank the National Center for Protein Sciences at Peking University in Beijing, China, for assistance with the high-performance liquid chromatography (HPLC; 1260 Infinity; Agilent, USA), microplate reader (SpectraMax M5), and confocal laser scanning microscopy (CLSM; A1R-si, Nikon, Japan). We thank Xiaodong Su Laboratory (School of Life Science, Peking University) for their help in the cell experiments.

## ■ REFERENCES

- (1) Fu, J. N.; Wang, X.; Yang, M.; Chen, Y. R.; Zhang, J. Y.; Deng, R. H.; Zhang, Z. N.; Yu, J. K.; Yuan, F. Z. Scaffold-Based Tissue Engineering Strategies for Osteochondral Repair. *Front Bioeng Biotechnol* **2022**, *9*, 812383.
- (2) Hunter, D. J.; Bierma-Zeinstra, S. Osteoarthritis. *Lancet* **2019**, *393* (10182), 1745–1759.
- (3) Briggs, A. M.; Woolf, A. D.; Dreinhofer, K.; Homb, N.; Hoy, D. G.; Kopansky-Giles, D.; Akesson, K.; March, L. Reducing the Global Burden of Musculoskeletal Conditions. *Bull. World Health Organ* **2018**, *96* (5), 366–368.
- (4) Ma, J.; Both, S. K.; Yang, F.; Cui, F. Z.; Pan, J.; Meijer, G. J.; Jansen, J. A.; van den Beucken, J. J. Concise Review: Cell-Based Strategies in Bone Tissue Engineering and Regenerative Medicine. *Stem Cells Transl Med.* **2014**, *3* (1), 98–107.
- (5) Mercado-Pagan, A. E.; Stahl, A. M.; Shanjani, Y.; Yang, Y. Vascularization in Bone Tissue Engineering Constructs. *Ann. Biomed Eng.* **2015**, *43* (3), 718–729.
- (6) Lyons, F. G.; Al-Munajjed, A. A.; Kieran, S. M.; Toner, M. E.; Murphy, C. M.; Duffy, G. P.; O'Brien, F. J. The Healing of Bony Defects by Cell-Free Collagen-Based Scaffolds Compared to Stem Cell-Seeded Tissue Engineered Constructs. *Biomaterials* **2010**, *31* (35), 9232–9243.
- (7) Lenas, P.; Moos, M.; Luyten, F. P. Developmental Engineering: A New Paradigm for the Design and Manufacturing of Cell-Based Products. Part I: From Three-Dimensional Cell Growth to Biomimetics of In Vivo Development. *Tissue Eng. Part B Rev.* **2009**, *15* (4), 381–394.

- (8) Lenas, P.; Moos, M.; Luyten, F. P. Developmental Engineering: A New Paradigm for the Design and Manufacturing of Cell-Based Products. Part II: From Genes to Networks: Tissue Engineering from the Viewpoint of Systems Biology and Network Science. *Tissue Eng. Part B Rev.* **2009**, *15* (4), 395–422.
- (9) Gerstenfeld, L. C.; Cullinane, D. M.; Barnes, G. L.; Graves, D. T.; Einhorn, T. A. Fracture Healing as a Post-Natal Developmental Process: Molecular, Spatial, and Temporal Aspects of Its Regulation. *Journal of cellular biochemistry* **2003**, *88* (5), 873–884.
- (10) Fu, R.; Liu, C.; Yan, Y.; Li, Q.; Huang, R. L. Bone Defect Reconstruction Via Endochondral Ossification: A Developmental Engineering Strategy. *J. Tissue Eng.* **2021**, *12*, 2041731421110042.
- (11) Sheehy, E. J.; Kelly, D. J.; O'Brien, F. J. Biomaterial-Based Endochondral Bone Regeneration: A Shift from Traditional Tissue Engineering Paradigms to Developmentally Inspired Strategies. *Mater. Today Bio* **2019**, *3*, 100009.
- (12) Thompson, E. M.; Matsiko, A.; Farrell, E.; Kelly, D. J.; O'Brien, F. J. Recapitulating Endochondral Ossification: A Promising Route to in Vivo Bone Regeneration. *J. Tissue Eng. Regen Med.* **2015**, *9* (8), 889–902.
- (13) Hall, B. K.; Miyake, T. All for One and One for All: Condensations and the Initiation of Skeletal Development. *Bioessays* **2000**, *22* (2), 138–147.
- (14) Caplan, A. I.; Correa, D. The Msc: An Injury Drugstore. *Cell Stem Cell* **2011**, *9* (1), 11–15.
- (15) Grayson, W. L.; Bunnell, B. A.; Martin, E.; Frazier, T.; Hung, B. P.; Gimple, J. M. Stromal Cells and Stem Cells in Clinical Bone Regeneration. *Nat. Rev. Endocrinol* **2015**, *11* (3), 140–150.
- (16) Li, Y. Y.; Lam, K. L.; Chen, A. D.; Zhang, W.; Chan, B. P. Collagen Microencapsulation Recapitulates Mesenchymal Condensation and Potentiates Chondrogenesis of Human Mesenchymal Stem Cells - a Matrix-Driven in Vitro Model of Early Skeletogenesis. *Biomaterials* **2019**, *213*, 119210.
- (17) Noonan, K. J.; Hunziker, E. B.; Nessler, J.; Buckwalter, J. A. Changes in Cell, Matrix Compartment, and Fibrillar Collagen Volumes between Growth-Plate Zones. *J. Orthop Res.* **1998**, *16* (4), 500–508.
- (18) Johnson, K.; Zhu, S.; Tremblay, M. S.; Payette, J. N.; Wang, J.; Bouchez, L. C.; Meeusen, S.; Althage, A.; Cho, C. Y.; Wu, X.; et al. A Stem Cell-Based Approach to Cartilage Repair. *Science* **2012**, *336* (6082), 717–721.
- (19) Kang, M. L.; Ko, J. Y.; Kim, J. E.; Im, G. I. Intra-Articular Delivery of Kartogenin-Conjugated Chitosan Nano/Microparticles for Cartilage Regeneration. *Biomaterials* **2014**, *35* (37), 9984–9994.
- (20) Teng, B.; Zhang, S.; Pan, J.; Zeng, Z.; Chen, Y.; Hei, Y.; Fu, X.; Li, Q.; Ma, M.; Sui, Y.; et al. A Chondrogenesis Induction System Based on a Functionalized Hyaluronic Acid Hydrogel Sequentially Promoting Hmsc Proliferation, Condensation, Differentiation, and Matrix Deposition. *Acta Biomater* **2021**, *122*, 145–159.
- (21) Lee, K. Y.; Mooney, D. J. Alginate: Properties and Biomedical Applications. *Prog. Polym. Sci.* **2012**, *37* (1), 106–126.
- (22) Lee, H. P.; Gu, L.; Mooney, D. J.; Levenston, M. E.; Chaudhuri, O. Mechanical Confinement Regulates Cartilage Matrix Formation by Chondrocytes. *Nat. Mater.* **2017**, *16* (12), 1243–1251.
- (23) Zhang, J.; Mujeeb, A.; Du, Y.; Lin, J.; Ge, Z. Probing Cell-Matrix Interactions in Rgd-Decorated Macroporous Poly (Ethylene Glycol) Hydrogels for 3d Chondrocyte Culture. *Biomed Mater.* **2015**, *10* (3), 035016.
- (24) Yang, L.; Tsang, K. Y.; Tang, H. C.; Chan, D.; Cheah, K. S. Hypertrophic Chondrocytes Can. Become Osteoblasts and Osteocytes in Endochondral Bone Formation. *Proc. Natl. Acad. Sci. U. S. A.* **2014**, *111* (33), 12097–12102.
- (25) Hu, D. P.; Ferro, F.; Yang, F.; Taylor, A. J.; Chang, W.; Miclau, T.; Marcucio, R. S.; Bahney, C. S. Cartilage to Bone Transformation During Fracture Healing Is Coordinated by the Invading Vasculature and Induction of the Core Pluripotency Genes. *Development* **2017**, *144* (2), 221–234.
- (26) Leslie-Barbick, J. E.; Saik, J. E.; Gould, D. J.; Dickinson, M. E.; West, J. L. The Promotion of Microvasculature Formation in Poly(Ethylene Glycol) Diacrylate Hydrogels by an Immobilized Vegf-Mimetic Peptide. *Biomaterials* **2011**, *32* (25), 5782–5789.
- (27) Su, J.; Satchell, S. C.; Wertheim, J. A.; Shah, R. N. Poly(Ethylene Glycol)-Crosslinked Gelatin Hydrogel Substrates with Conjugated Bioactive Peptides Influence Endothelial Cell Behavior. *Biomaterials* **2019**, *201*, 99–112.
- (28) Hung, B. P.; Gonzalez-Fernandez, T.; Lin, J. B.; Campbell, T.; Lee, Y. B.; Panitch, A.; Alsberg, E.; Leach, J. K. Multi-Peptide Presentation and Hydrogel Mechanics Jointly Enhance Therapeutic Duo-Potential of Entrapped Stromal Cells. *Biomaterials* **2020**, *245*, 119973.
- (29) Sun, L.; Ma, Y.; Niu, H.; Liu, Y.; Yuan, Y.; Liu, C. Recapitulation of in Situ Endochondral Ossification Using an Injectable Hypoxia-Mimetic Hydrogel. *Adv. Funct. Mater.* **2021**, *31* (5), 2008515.
- (30) Liu, Y.; Yang, Z.; Wang, L.; Sun, L.; Kim, B. Y. S.; Jiang, W.; Yuan, Y.; Liu, C. Spatiotemporal Immunomodulation Using Biomimetic Scaffold Promotes Endochondral Ossification-Mediated Bone Healing. *Adv. Sci. (Weinh)* **2021**, *8* (11), e2100143.
- (31) Rowley, J. A.; Madlambayan, G.; Mooney, D. J. Alginate Hydrogels as Synthetic Extracellular Matrix Materials. *Biomaterials* **1999**, *20* (1), 45–53.
- (32) Scotti, C.; Tonnarelli, B.; Papadimitropoulos, A.; Scherberich, A.; Schaefer, S.; Schauerte, A.; Lopez-Rios, J.; Zeller, R.; Barbero, A.; Martin, I. Recapitulation of Endochondral Bone Formation Using Human Adult Mesenchymal Stem Cells as a Paradigm for Developmental Engineering. *Proc. Natl. Acad. Sci. U. S. A.* **2010**, *107* (16), 7251–7256.
- (33) Grogan, S. P.; Barbero, A.; Winkelmann, V.; Rieser, F.; Fitzsimmons, J. S.; O'Driscoll, S.; Martin, I.; Mainil-Varlet, P. Visual Histological Grading System for the Evaluation of in Vitro-Generated Neocartilage. *Tissue Eng.* **2006**, *12* (8), 2141–2149.
- (34) Dong, Y.; Sun, X.; Zhang, Z.; Liu, Y.; Zhang, L.; Zhang, X.; Huang, Y.; Zhao, Y.; Qi, C.; Middleley, A. C.; et al. Regional and Sustained Dual-Release of Growth Factors from Biomimetic Tri-layered Scaffolds for the Repair of Large-Scale Osteochondral Defects. *Applied Materials Today* **2020**, *19*, 100548.
- (35) Luo, Z.; Pan, J.; Sun, Y.; Zhang, S.; Yang, Y.; Liu, H.; Li, Y.; Xu, X.; Sui, Y.; Wei, S. Injectable 3d Porous Micro-Scaffolds with a Bio-Engine for Cell Transplantation and Tissue Regeneration. *Adv. Funct. Mater.* **2018**, *28* (41), 1804335.
- (36) Luo, Z.; Liu, Z.; Liang, Z.; Pan, J.; Xu, J.; Dong, J.; Bai, Y.; Deng, H.; Wei, S. Injectable Porous Microchips with Oxygen Reservoirs and an Immune-Niche Enhance the Efficacy of Car T Cell Therapy in Solid Tumors. *ACS Appl. Mater. Interfaces* **2020**, *12* (51), S6712–S6722.
- (37) Liu, J.; Yu, C.; Chen, Y.; Cai, H.; Lin, H.; Sun, Y.; Liang, J.; Wang, Q.; Fan, Y.; Zhang, X. Fast Fabrication of Stable Cartilage-Like Tissue Using Collagen Hydrogel Microsphere Culture. *J. Mater. Chem. B* **2017**, *5* (46), 9130–9140.
- (38) Annabi, N.; Nichol, J. W.; Zhong, X.; Ji, C.; Koshy, S.; Khademhosseini, A.; Dehghani, F. Controlling the Porosity and Microarchitecture of Hydrogels for Tissue Engineering. *Tissue Eng. Part B Rev.* **2010**, *16* (4), 371–383.
- (39) Tsou, Y. H.; Khoneisser, J.; Huang, P. C.; Xu, X. Hydrogel as a Bioactive Material to Regulate Stem Cell Fate. *Bioact Mater.* **2016**, *1* (1), 39–55.
- (40) Ambrosch, K.; Manhardt, M.; Loth, T.; Bernhardt, R.; Schulz-Siegmund, M.; Hacker, M. C. Open Porous Microscaffolds for Cellular and Tissue Engineering by Lipid Templating. *Acta Biomater* **2012**, *8* (3), 1303–1315.
- (41) Martin, Y.; Eldardiri, M.; Lawrence-Watt, D. J.; Sharpe, J. R. Microcarriers and Their Potential in Tissue Regeneration. *Tissue Eng. Part B Rev.* **2011**, *17* (1), 71–80.
- (42) Pedram, P.; Mazio, C.; Imparato, G.; Netti, P. A.; Salerno, A. Bioinspired Design of Novel Microscaffolds for Fibroblast Guidance toward in Vitro Tissue Building. *ACS Appl. Mater. Interfaces* **2021**, *13* (8), 9589–9603.
- (43) Karageorgiou, V.; Kaplan, D. Porosity of 3d Biomaterial Scaffolds and Osteogenesis. *Biomaterials* **2005**, *26* (27), S474–S491.

- (44) Luo, Z.; Deng, Y.; Zhang, R.; Wang, M.; Bai, Y.; Zhao, Q.; Lyu, Y.; Wei, J.; Wei, S. Peptide-Laden Mesoporous Silica Nanoparticles with Promoted Bioactivity and Osteo-Differentiation Ability for Bone Tissue Engineering. *Colloids Surf, B* **2015**, *131*, 73–82.
- (45) Wu, S.; Peng, H.; Li, X.; Streubel, P. N.; Liu, Y.; Duan, B. Effect of Scaffold Morphology and Cell Co-Culture on Tenogenic Differentiation of Hadmsc on Centrifugal Melt Electrospun Poly (Lactic Acid) Fibrous Meshes. *Biofabrication* **2017**, *9* (4), 044106.
- (46) Mitrousis, N.; Fokina, A.; Shoichet, M. S. Biomaterials for Cell Transplantation. *Nature Reviews Materials* **2018**, *3* (11), 441–456.
- (47) Petersen, A.; Princ, A.; Korus, G.; Ellinghaus, A.; Leemhuis, H.; Herrera, A.; Klaumunzer, A.; Schreivogel, S.; Woloszyk, A.; Schmidt-Bleek, K.; et al. A Biomaterial with a Channel-Like Pore Architecture Induces Endochondral Healing of Bone Defects. *Nat. Commun.* **2018**, *9* (1), 4430.
- (48) Villanueva, I.; Weigel, C. A.; Bryant, S. J. Cell-Matrix Interactions and Dynamic Mechanical Loading Influence Chondrocyte Gene Expression and Bioactivity in Peg-Rgd Hydrogels. *Acta Biomater* **2009**, *5* (8), 2832–2846.
- (49) Lee, J.; Jeon, O.; Kong, M.; Abdeen, A. A.; Shin, J. Y.; Lee, H. N.; Lee, Y. B.; Sun, W.; Bandaru, P.; Alt, D. S.; et al. Combinatorial Screening of Biochemical and Physical Signals for Phenotypic Regulation of Stem Cell-Based Cartilage Tissue Engineering. *Sci. Adv.* **2020**, *6* (21), eaaz5913.
- (50) Kronenberg, H. M. Developmental Regulation of the Growth Plate. *Nature* **2003**, *423* (6937), 332–336.
- (51) SundarRaj, N.; Fite, D.; Ledbetter, S.; Chakravarti, S.; Hassell, J. R. Perlecan Is a Component of Cartilage Matrix and Promotes Chondrocyte Attachment. *J. Cell Sci.* **1995**, *108* (7), 2663–2672.
- (52) Kim, I. L.; Khetan, S.; Baker, B. M.; Chen, C. S.; Burdick, J. A. Fibrous Hyaluronic Acid Hydrogels That Direct Msc Chondrogenesis through Mechanical and Adhesive Cues. *Biomaterials* **2013**, *34* (22), 5571–5580.
- (53) Tsang, K. Y.; Chan, D.; Cheah, K. S. Fate of Growth Plate Hypertrophic Chondrocytes: Death or Lineage Extension. *Dev Growth Differ* **2015**, *57* (2), 179–192.
- (54) Pelttari, K.; Winter, A.; Steck, E.; Goetzke, K.; Hennig, T.; Ochs, B. G.; Aigner, T.; Richter, W. Premature Induction of Hypertrophy During in Vitro Chondrogenesis of Human Mesenchymal Stem Cells Correlates with Calcification and Vascular Invasion after Ectopic Transplantation in Scid Mice. *Arthritis Rheum* **2006**, *54* (10), 3254–3266.
- (55) Qin, X.; Jiang, Q.; Nagano, K.; Moriishi, T.; Miyazaki, T.; Komori, H.; Ito, K.; Mark, K. V.; Sakane, C.; Kaneko, H.; et al. Runx2 Is Essential for the Transdifferentiation of Chondrocytes into Osteoblasts. *PLoS Genet* **2020**, *16* (11), e1009169.
- (56) Bonnelye, E.; Chabadel, A.; Saltel, F.; Jurdic, P. Dual Effect of Strontium Ranelate: Stimulation of Osteoblast Differentiation and Inhibition of Osteoclast Formation and Resorption in Vitro. *Bone* **2008**, *42* (1), 129–138.
- (57) Wilusz, R. E.; Sanchez-Adams, J.; Guilak, F. The Structure and Function of the Pericellular Matrix of Articular Cartilage. *Matrix Biol.* **2014**, *39*, 25–32.
- (58) Pigeot, S.; Klein, T.; Gullotta, F.; Dupard, S. J.; Garcia Garcia, A.; Garcia-Garcia, A.; Prithiviraj, S.; Lorenzo, P.; Filippi, M.; Jaquier, C.; et al. Manufacturing of Human Tissues as Off-the-Shelf Grafts Programmed to Induce Regeneration. *Adv. Mater.* **2021**, *33* (43), e2103737.
- (59) Yu, Y.; Park, Y. S.; Kim, H. S.; Kim, H. Y.; Jin, Y. M.; Jung, S. C.; Ryu, K. H.; Jo, I. Characterization of Long-Term in Vitro Culture-Related Alterations of Human Tonsil-Derived Mesenchymal Stem Cells: Role for Ccn1 in Replicative Senescence-Associated Increase in Osteogenic Differentiation. *J. Anat* **2014**, *225* (5), 510–518.
- (60) Bertolo, A.; Mehr, M.; Janner-Jametti, T.; Graumann, U.; Aebli, N.; Baur, M.; Ferguson, S. J.; Stoyanov, J. V. An in Vitro Expansion Score for Tissue-Engineering Applications with Human Bone Marrow-Derived Mesenchymal Stem Cells. *J. Tissue Eng. Regen Med.* **2016**, *10* (2), 149–161.
- (61) Yang, Y. K.; Ogando, C. R.; Wang See, C.; Chang, T. Y.; Barabino, G. A. Changes in Phenotype and Differentiation Potential of Human Mesenchymal Stem Cells Aging in Vitro. *Stem Cell Res. Ther* **2018**, *9* (1), 131.
- (62) Barbero, A.; Grogan, S.; Schafer, D.; Heberer, M.; Mainil-Varlet, P.; Martin, I. Age Related Changes in Human Articular Chondrocyte Yield, Proliferation and Post-Expansion Chondrogenic Capacity. *Osteoarthritis Cartilage* **2004**, *12* (6), 476–484.